The BRCA1-BARD1 complex associates with the synaptonemal complex and pro-crossover factors and influences RAD-51 dynamics during *Caenorhabditis elegans* meiosis

Eva Janisiw[1,2], Maria Rosaria Dello Stritto[1], Verena Jantsch[1] and Nicola Silva[1]*

[1] Department of Chromosome Biology, Max F. Perutz Laboratories, University of Vienna, Vienna BioCenter, 1030 Vienna, Austria.

[2] Present address: Centre for Anatomy and Cell Biology, Medical University of Vienna, 1090 Vienna, Austria.

* Corresponding author

E-mail: nicola.silva@univie.ac.at

Short title: BRCA1-BARD1 interact with the synaptonemal complex and crossover factors

Key words: *C. elegans* meiosis, BRC-1, BRD-1, DNA damage, meiotic DNA repair

Abstract

During meiosis, the maternal and paternal homologous chromosomes must align along their entire length and recombine to achieve faithful segregation in the gametes. Meiotic recombination is accomplished through the formation of DNA double-strand breaks, a subset of which can mature into crossovers to link the parental homologous chromosomes and promote their segregation. Breast and ovarian cancer susceptibility protein BRCA1 and its heterodimeric partner BARD1 play a pivotal role in DNA repair in mitotic cells; however, their functions in gametogenesis are less well understood. Here we show that localization of BRC-1 and BRD-1 (*Caenorhabditis elegans* orthologues of BRCA1 and BARD1) is dynamic during meiotic prophase I; they ultimately becoming concentrated at regions surrounding the presumptive crossover sites, co-localizing with the pro-crossover factors COSA-1, MSH-5 and ZHP-3. The synaptonemal complex is essential for BRC-1 loading onto chromosomes but recombination is not. BRC-1 forms an in vivo complex with the synaptonemal complex component SYP-3 and the crossover-promoting factor MSH-5. Furthermore, BRC-1 is essential for efficient stage-specific recruitment of the RAD-51 recombinase to DNA damage sites when synapsis is impaired and upon induction of exogenous DNA double-strand breaks. Taken together, our data provide new insights into the localization and meiotic function of the BRC-1–BRD-1 complex and highlight their essential role in DNA double-strand break repair during gametogenesis.

Author summary

Sexually reproducing species rely on meiosis to transmit their genetic information across generations. Parental chromosomes (homologues) undergo many distinctive processes in their complex journey from attachment to segregation. The physiological induction of DNA double strand breaks is crucial for promoting correct chromosome segregation: they are needed to activate the DNA repair machinery responsible for creating physical connections, or crossovers (COs), between the homologues. In turn, crossovers promote the accurate segregation of the chromosomes in daughter cells. The BRCA1–BARD1 complex has a pivotal role during DNA repair in somatic cells and is exclusively located on unaligned chromosomal regions during mammalian meiosis. We show that in *Caenorhabditis elegans*, BRCA1 and BARD1 localize to chromosomes at all stages of meiotic prophase I and are enriched at presumptive crossover sites. We found that BRCA1 promotes DNA loading of the repair factor RAD-51 in specific mutant backgrounds and upon exogenous damage induction. Our data provide evidence for a direct physical association between BRCA1 and pro-crossover factors (including the synaptonemal complex) and identify an important role for BRCA1 in stimulating meiotic DNA repair. Further studies are necessary to identify the substrates acted upon by BRCA1–BARD1 complex to maintain genome stability in the gametes.

63 # Introduction

64 The genetic information encoded by DNA must be accurately copied and transmitted from
65 one generation to the next. In somatic cells, DNA is duplicated and equally partitioned into
66 daughter cells via mitosis, whereas in germ cells, which give rise to gametes, chromosome
67 segregation relies on meiosis, a specialized cell division mechanism which produces haploid
68 cells from diploid progenitors. Meiosis requires a unique programme of finely regulated
69 events before cell division to accomplish faithful chromosome segregation. Cognate paternal
70 and maternal chromosomes (homologous chromosomes) find each other (homologous
71 pairing) and then fully align; the interaction is stabilized by formation of the synaptonemal
72 complex (SC). Ultimately, exchange of DNA (recombination) between the homologues
73 chromosomes establishes physical connections, which are essential for faithful segregation
74 (1, 2).
75
76 The *Caenorhabditis elegans* gonad is a powerful system for studying chromosomes during
77 both mitosis and meiosis because of the cytological accessibility and the spatio-temporal
78 organization of nuclei into all prophase I stages (3). Morphological changes to chromosomes
79 mark the engagement of key steps in meiotic progression. At meiotic onset, chromatin adopts
80 a clustered, "half-moon" shape, reflecting chromosome movement and reorganization (4-6).
81 This structure marks the transition zone (corresponding to the leptotene–zygotene stages).
82 Once homologues are aligned, a tripartite proteinaceous structure called synaptonemal
83 complex (SC) is formed between each homologue pair to allow genetic exchange during CO-
84 dependent DNA repair (1, 2, 7-10). DNA recombination is initiated by the deliberate
85 induction of DNA double-strand breaks (DSBs) by the topoisomerase II-like enzyme, SPO-
86 11 (11, 12). In all species, the number of DSBs largely exceeds the final number of COs,
87 suggesting that many DSBs are repaired via pathways such as inter-sister repair (IS) or

synthesis-dependent strand annealing (13). In *C. elegans*, only one CO is formed between each homologous pair (14), and this depends on the function of the MSH-4/MSH-5 heterodimer (orthologues of the yeast and mammalian MutSγ complex components, MSH4/MSH5) (15-18), the cyclin COSA-1 (orthologue of mammalian CNTD1) (19, 20) and the E3 SUMO-ligase ZHP-3 (orthologue of yeast Zip3) (21-23). CO formation is abolished in absence of DSBs (e.g. in *spo-11* mutants) or synapsis; however, unlike in other model systems, lack of DNA breaks does not prevent SC formation in *C. elegans* (7, 11). Meiotic DSB repair also relies on RAD-51-mediated repair in *C. elegans* (24, 25): the RAD-51 recombinase localizes to discrete chromatin-associated foci starting in the transition zone and peaking in early pachytene; RAD-51 disengages from DNA in mid-pachytene (7). Markers of aberrant RAD-51 loading, such as increased foci number and/or extended accumulation, are bona fide indicators of defective DSB processing and recombination. CO induction triggers reorganization of the SC components into distinct domains on bivalents (pairs of homologous chromosomes held together by a chiasma): the central elements are confined to the short arm (containing the CO) and the axial elements to the long arm (26-30). This reorganization is particularly evident during diplotene, at which stage bivalents progressively condense and appear as six DAPI-stained bodies in diakinesis nuclei, which are a read-out for the successful execution of prophase I events (aberrant structures include achiasmatic chromosomes (univalents) or fused/fragmented chromatin masses (11, 16, 31)).

The breast and ovarian cancer susceptibility protein BRCA1 and its obligate heterodimeric partner BARD1 form an E3 ubiquitin ligase module (the BCD complex), the functions of which have been extensively studied in mitotic cells (32). The BRCA1–BARD1 heterodimer promotes homologous recombination (HR) during the S–G2 stages, by both favouring extended DNA break resection and preventing the non-homologous end joining (NHEJ)-

113 promoting factor 53BP1 (33) from binding to the site of ongoing DNA repair. It also
114 enhances BRCA2 and RAD51 loading at DNA damage sites to elicit accurate DNA repair
115 (32). *BRCA1*-null mutants are embryonic lethal, thus hindering the study of this factor in
116 gametogenesis (34-44). Mutants containing hypomorphic and gain-of-function alleles show
117 increased apoptotic cell death during spermatogenesis, as well as reduced loading of the pro-
118 CO factor MSH4 and a severe delay in MLH1 focus formation during oogenesis (45). *C.*
119 *elegans brc-1*/BRCA1 mutants are viable and fertile, albeit with increased DNA damage-
120 dependent apoptosis during oogenesis and SPO-11-dependent accumulation of RAD-51 foci,
121 suggesting a defect in processing meiotic recombination intermediates (46, 47). Importantly,
122 blocking *brc-1* function in CO-defective mutants leads to the formation of aberrant chromatin
123 bodies in diakinesis nuclei, underscoring the importance of BRC-1 in the IS repair pathway
124 (47).
125
126 Here we report that in the *C. elegans* germline, unlike in mammalian systems, BRC-1 and
127 BRD-1 are abundantly expressed throughout meiotic prophase I and display a dynamic
128 localization pattern in germ cells, switching from nucleoplasmic expression in early meiotic
129 stages to SC association in pachytene, where they become progressively enriched at
130 chromosome subdomains bearing the CO sites. We provide in vivo evidence that BRC-1
131 forms a complex with both MSH-5 and the SC central element, SYP-3. Localization of BRC-
132 1 and BRD-1 in germ cells is differently regulated by synapsis and CO formation. Finally, we
133 show that BRC-1 promotes stage-specific RAD-51 loading when SC formation is impaired
134 and upon exogenous DNA damage induction. Similar findings are reported by Li and
135 colleagues in the accompanying manuscript. Taken together, our data highlight the multiple
136 functions of the BRC-1–BRD-1 heterodimer during gametogenesis.
137

Results

BRC-1 and BRD-1 display a dynamic localization pattern in the germline and are recruited to the short arm of the bivalent

To gain insight into BRC-1 and BRD-1 function during gametogenesis, we analysed their localization patterns during meiotic prophase I. To this end, we tagged the endogenous *brc-1* locus with a 3′ HA tag using a CRISPR/Cas9 approach (48, 49) and detected BRD-1 using a previously characterized specific antibody (46, 50). BRC-1::HA protein function was assessed by exposing the tagged animals to ionizing radiation (IR): as previously reported (46), *brc-1* mutants were sterile, whereas *brc-1*::*HA* worms responded to IR in a similar way to wild-type animals, thus proving that the tagged protein is fully functional (Fig 1A). Using a recently published method for isolating germline-enriched proteins (51) involving protein fractionation and western blot analysis, we showed that BRC-1::HA is enriched in the nucleus: most was in the soluble nuclear pool fraction and a smaller proportion was chromatin bound (Fig 1B). Interestingly, unlike in whole-cell extracts, BRC-1::HA was detected as a doublet in fractionated samples, suggesting that a less abundant isoform becomes detectable after enrichment with this extraction method or perhaps the presence of a post-translational modification.

Previous reports indicate that during mouse meiosis, BRCA1 localizes to nascent SC elements during the leptotene/zygotene stages; in pachytene cells, it is exclusively located at asynapsed region of the XY-sex body during spermatogenesis or on asynapsed chromosomes during oocyte meiosis (52-54). In contrast, in the *C. elegans* germline both BRC-1 and BRD-1 were expressed in all nuclei during meiotic prophase I (Figs 1C and S1A) and, as expected, largely co-localized (Fig 1D). As observed in mammalian models, BRC-1 and BRD-1 loading is interdependent in nematodes: *brc-1* mutant germlines did not display any BRD-1

163 staining (Fig S1B) (55-57). Intriguingly, at the transition between mid to late pachytene,
164 BRC-1 and BRD-1 staining switched from a rather diffuse to a discrete linear pattern along
165 the chromosomes; in late pachytene nuclei, BRC-1 and BRD-1 progressively retracted into
166 six short "comet-like" structures (Figs 1C, D and S1A), a specific pattern indicating
167 localization to both CO sites and the short arm of bivalent (7, 8, 21, 22, 58, 59). To assess
168 whether the BCD complex is indeed recruited to the short arm of the bivalent, we co-stained
169 *brc-1*::*HA* germ lines with antibodies directed against the central element of the SC, SYP-1
170 (8) and the axial protein HTP-3 (60). As shown in Fig 2A, BRC-1 co-localized with SYP-1 in
171 late pachytene/diplotene nuclei, confirming that the BCD complex becomes gradually
172 concentrated in the region surrounding the CO site. Strikingly, BRC-1 enrichment at discrete
173 regions preceded SYP-1 localization to the short arm of the bivalent (six robust stretches
174 were seen only at late pachytene/diplotene stage). At meiosis onset, the PLK-2 polo-like
175 kinase is enriched at the nuclear envelope attachment sites of chromosome ends, where it
176 promotes homologous pairing and synapsis (61, 62). In late pachytene, PLK-2 re-locates to
177 discrete domains along the SC, marking local enrichment of recombination factors (63).
178 PLK-2 redistribution also occurs before SYP-1 redistribution to the short arm and influences
179 the SC structure (63, 64). Given that BRC-1 redistribution had similar kinetics, we co-stained
180 PLK-2 and BRC-1 (Fig 2B) and found that regions enriched for BRC-1 fully overlapped with
181 the PLK-2 staining pattern in late pachytene and diplotene. Thus, the BCD complex is
182 ubiquitously expressed during meiotic prophase I and becomes progressively enriched on the
183 short arm of the bivalent prior to SYP-1 recruitment, where it co-localizes with PLK-2.
184

185 **CO establishment triggers redistribution of the BRC-1–BRD-1 complex**

186 In *C. elegans*, formation of inter-homologue COs depends on several proteins, such as the
187 COSA-1 cyclin (20), the MutSγ heterodimer, MSH4/MSH-5 (15, 16) and the ZHP-3 E3

188 SUMO-ligase (22). MSH-5 and ZHP-3 are detected at early meiotic stages, with the former
189 accumulating in many foci (these are probably recombination intermediates with both CO
190 and non-CO (NCO) outcomes) and the latter localizing along the SC (20-22). COSA-1 is
191 prominently detected at mid–late pachytene transition as six foci (one CO for each
192 homologue pair), which also contain MSH-5 and ZHP-3 (20). Since we observed BRC-1 and
193 BRD-1 recruitment to the short arm of bivalents (chromosome subdomains caused by the
194 formation of CO intermediates (26, 27, 29)), we wondered whether local enrichment of the
195 BCD complex coincides with the regions labelled with pro-CO factors. Comparison of the
196 localization dynamics of GFP::COSA-1 and BRC-1::HA showed that BRC-1 starts to
197 become concentrated concomitantly with enhanced COSA-1 loading and defines a discrete
198 area which later also contains SYP-1 (Fig 3A). We obtained the same localization pattern by
199 monitoring BRD-1 loading (Fig S2). Furthermore, staining with anti-ZHP-3 antibody (21)
200 also revealed full co-localization of ZHP-3 with BRC-1 (Fig 3A). To evaluate BRC-1 co-
201 localization with MSH-5, we first added a 5′ GFP tag to the endogenous *msh-5* locus with
202 CRISPR/Cas9. The tagged line was fully functional, with no defects in chiasmata formation
203 (not shown), suggesting that GFP::MSH-5 is competent to promote CO formation. Similar to
204 ZHP-3 and COSA-1, BRC-1::HA was enriched at defined regions containing a single
205 GFP::MSH-5 focus, which also labels the CO site (Fig 3B). We performed structured
206 illumination microscopy to further analyse BRC-1 association with the CO site. For this, we
207 added a 5′ OLLAS tag to the endogenous *cosa-1* locus (65, 66). This fully functional line was
208 crossed into *brc-1*::*HA* worms and co-stained for OLLAS (COSA-1), BRC-1 and SYP-1.
209 This further confirmed BRC-1 enrichment around COSA-1-labelled CO sites; however, in
210 these nuclei BRC-1 decorates the region of the SC embracing the putative recombination site;
211 thus, it appears to surround, rather than overlapping with, COSA-1 (Fig 3C).
212

To assess whether BRC-1–BRD-1 redistribution depends on CO establishment, we generated a *brc-1*::*HA*; *spo-11* mutant strain to monitor BRC-1::HA loading in absence of meiotic DSBs, which are essential for inducing CO formation. A previous report showed that in *spo-11* mutants COSA-1 occasionally forms very few foci (possibly arising from mitotic or spontaneous DSBs) and ZHP-3 remains localized along the SC without forming retraction "comets" due to a lack of chiasmata (20). In *spo-11* mutants, BRC-1 remained co-localized with ZHP-3 along the SC, without redistributing to chromosome subdomains. This confirms that BRC-1 redistribution depends on chiasmata formation (Fig 3D).

Exogenous DSB induction is sufficient to temporarily restore COSA-1 loading and therefore chiasmata formation in *spo-11* mutants (11, 20, 64). Thus, we investigated whether γ-irradiation could rescue the failure in BRC-1 redistribution. We exposed *brc-1*::*HA; spo-11* mutant worms to 20 Gy and analysed BRC-1 and ZHP-3 loading at 8 hours post irradiation: at this time point, all late pachytene nuclei in *spo-11* mutants display six COSA-1 foci, suggesting that CO induction is fully rescued (20). In the irradiated samples, ZHP-3 was retracted towards the CO site and, consistent with this, BRC-1 also became concentrated around the CO site (Fig 3E). Based on these data, we conclude that BRC-1 and BRD-1 localize to the short arms of bivalents and that their reorganization in mid-pachytene nuclei is dependent on CO establishment.

BRC-1 physically interacts with MSH-5 and SYP-3 in vivo

Given its spatial association with both CO factors and the SC, we wondered whether BRC-1 formed protein complexes with these factors in vivo. We performed pull-down experiments using the *brc-1*::*HA; GFP*::*msh-5* strain (Fig 3) and crossed *brc-1*::*HA* into worms expressing a single-copy insertion transgene encoding a largely functional GFP::SYP-3 protein (67). Worms from both strains were used to generate cytosolic, soluble nuclear and chromatin-

bound protein fractions (51): both nuclear fractions were pooled for immunoprecipitation experiments. Immunoprecipitation of GFP::MSH-5 and GFP::SYP-3 from *brc-1*::*HA; GFP*::*msh-5* and *syp-3; [GFP*::*syp-3]; brc-1*::*HA* strains, respectively, followed by western blot analysis with anti-HA antibodies revealed that that BRC-1::HA was present in both samples (Fig 3F). This suggests that BRC-1 forms a complex with both MSH-5 and SYP-3 proteins in vivo. Thus, we identified a previously unknown physical interaction of the BCD complex with the pro-CO factor MSH-5 and the SC central element SYP-3, highlighting a possible role for BRC-1–BRD-1 at the interface between synapsis and recombination.

Synapsis and recombination have different effects on BRC-1 and BRD-1 loading

Given that CO establishment triggers BRC-1–BRD-1 redistribution (Fig 3C, D), we sought to analyse their localization in mutants that have impairment at different steps of CO formation. As already mentioned, an absence of DSBs leads to a lack of recombination, which prevents BRC-1 and BRD-1 retraction to the short arms of bivalents. We therefore asked whether impaired DNA repair by HR, but not by DSB induction, influences BRC-1 and BRD-1 localization. To address this, we crossed *brc-1*::*HA* into the *msh-5* mutant, which cannot convert recombination intermediates into mature CO products (7, 16). In *msh-5* mutants, BRC-1 accumulated along the SC but retraction was not observed (Fig 4A), similar to the localization pattern observed in *spo-11* (Fig 3). Then, we analysed BRC-1::HA staining in *rad-51* mutants, which have normal SC assembly but no homologous DNA repair due to lack of RAD-51-dependent strand displacement and invasion of the homologous chromosome (24, 25). Interestingly, BRC-1 had a rather punctate staining pattern, perhaps through labelling recombination-independent DNA joined molecules (Fig 4A). Despite this, a strong association with SYP-1 in chromosome subdomains was observed in nuclei exiting the pachytene stage (we also observed this in *msh-5* mutants). We observed a similar pattern of

BRD-1 localization in *com-1* mutants (Fig S3): here, interfering with DSB resection impairs RAD-51 loading and therefore abolishes CO formation (68). These results suggest that a lack of COs per se impairs redistribution of the BCD complex in late pachytene cells without perturbing loading along the SC. However, in mutants such as *rad-51* that are defective in the early steps of recombination, BRC-1–BRD-1 association with the SC is also dramatically reduced. Next, we sought to analyse whether BRC-1 and BRD-1 loading is regulated by synapsis. We analysed BRC-1::HA loading in the complete and partial absence of SC, as well as in mutants in which synapsis occurs between non-homologous chromosomes. The central portion of the SC is formed by several proteins (SYP-1–4) which are loaded in an interdependent manner; thus, all are necessary to establish synapsis (7, 8, 58, 59). In the *syp-2* synapsis-null mutant (7), BRC-1::HA had a rather punctate staining pattern throughout meiotic prophase I. Strikingly, unlike in the wild type, where BRC-1 starts to spread along the SC immediately after the disappearance of RAD-51, in *syp-2* mutants BRC-1 foci remained in close proximity to and co-localized with RAD-51 foci in mid and late pachytene nuclei (Fig 4B). In *C. elegans*, a family of zinc-finger nuclear proteins connects chromosome-specific ends (i.e. pairing centres) to the nuclear envelope to promote chromosome pairing and synapsis (69, 70). ZIM-2 and HIM-8 bind to the ends of chromosomes V and X, respectively. Therefore, chromosome V is asynapsed in *zim-2* mutants and chromosome X is asynapsed in *him-8* mutants. We asked whether a partial deficiency in synapsis establishment (affecting only one chromosome pair) also changes BRC-1 loading dynamics. Analysis of BRC-1::HA expression in *him-8* and *zim-2* mutants revealed a lack of BRC-1 on unsynapsed chromosomes pairs, despite normal loading along the SC and retraction towards the CO site in the remaining bivalents (Fig 4C,D), suggesting that local synapsis defects do not impair BRC-1 loading. Lastly, we analysed BRD-1 loading in two mutants with deregulated SC assembly. HTP-1 is a HORMA-domain-containing

protein essential to prevent SC assembly between non-homologous chromosomes and PROM-1 is an F-box protein involved in promoting meiotic entry and homologous pairing. Both *htp-1* and *prom-1* mutants display extensive SYP-1 loading between non-homologous chromosomes as well as asynapsed chromosome regions; consequentially, chiasmata formation is severely impaired (26, 71). Remarkably, the degree of BRD-1 co-localization with SYP-1 was extremely reduced in both *htp-1* and *prom-1* mutants, with most BRD-1 detected as bright agglomerates within the nucleus (Fig S4). Thus, we conclude that BRC-1 and BRD-1 redistribution during meiotic progression requires CO establishment and is tightly regulated by SCs.

BRC-1 promotes RAD-51 recruitment in the absence of synapsis

BRC-1 is dispensable for establishing synapsis and chiasmata; however, *brc-1* mutant germlines have a higher number of and more persistent RAD-51-labelled recombination intermediates compared with the wild type (Fig S5) (46, 47). Impaired BRC-1 localization, and probably also impaired function, in CO-defective mutants leads to the formation of abnormal chromosome structures in diakinesis nuclei, possibly due to deficient IS repair (47). DSB repair during meiosis is channelled into both CO and NCO pathways. Since it has been suggested that BRC-1 might preferentially function in NCOs (47), we investigated whether other factors involved in resolving the recombination intermediates required for both CO and NCO repair might also be affected. In somatic cells, the RTR complex mediates efficient resolution of recombination intermediates by promoting the dissolution of double Holliday junctions to yield non-CO products (72-74). RMI1 is an essential component of the RTR complex and a scaffolding component for other complex members, BLM and TOP3A, which promotes their dissolution activity (74). The *C. elegans* RMI1orthologue, RMH-1, localizes to recombination foci during meiosis: it appears in early pachytene and peaks in mid-

pachytene, accumulating in many foci and possibly labelling all recombination intermediates. At late pachytene transition, the number of RMH-1 foci is reduced to roughly six per nucleus; these foci co-localize with foci of the pro-CO factors COSA-1, MSH-5 and ZHP-3. Lack of RMH-1 causes a drastic reduction in chiasmata formation due to impaired COSA-1 and MSH-5 loading. However, in CO-deficient backgrounds such as *cosa-1*, *msh-5* and *zhp-3* mutants, RMH-1 is still recruited in early pachytene but is not retained until late pachytene. Therefore, it has been postulated that RMH-1 functions in both the CO and NCO pathways (75). MSH-5 displays a similar localization, but does not fully co-localize with RMH-1 (20, 75). We scored COSA-1, MSH-5 and RMH-1 nuclear localization in *brc-1* mutants in nuclei spanning the transition zone to late pachytene stage. Interestingly, GFP::MSH-5 accumulation was reduced in early and mid-pachytene, with a similar, but less prominent, trend for GFP::RMH-1 (Fig 5A,B). By late pachytene, both proteins had been recruited into six foci, together with COSA-1, suggesting that the early processing of recombination intermediates might be defective in absence of BRC-1.

Given that BRC-1 and BRD-1 loading are regulated by synapsis and the establishment of COs, and that a lack of BRC-1 might affect the processing of NCOs rather than COs, we next assessed the effects of BRC-1 depletion in genetic backgrounds defective in chiasmata formation, which hence rely solely on NCOs to repair meiotic DSBs. We first analysed DAPI-stained bodies in diakinesis nuclei from *cosa-1 brc-1* and *brc-1; syp-2* double mutants to confirm the presence of aberrant chromatin structures (Fig 6A), as previously reported (46, 47). As abnormalities in diakinesis nuclei can result from impaired RAD-51-dependent repair of meiotic DSBs (24, 31, 76), we sought to analyse whether lack of *brc-1* altered RAD-51 dynamics. To this end, we quantified RAD-51 in *cosa-1 brc-1* and *brc-1; syp-2* mutants. Failure to convert recombination intermediates into mature CO products has been linked to

increased RAD-51 levels and its delayed removal during meiotic prophase due to either excessive DSB induction or slower processing of recombination intermediates (5, 6, 15, 16), which are eventually channelled into alternative repair pathways (e.g. IS repair) (7). In fact, both *cosa-1* and *syp-2* mutants accumulated high levels of RAD-51, which disengaged from chromatin in mid and late pachytene, respectively (Fig 6B, C) (7, 20). Remarkably, removal of BRC-1 from *cosa-1* and *syp-2* mutants had different effects on RAD-51 dynamics: in both *cosa-1 brc-1* and *brc-1; syp-2* double mutants, there were far fewer RAD-51 foci in early pachytene compared with both single mutants; however, in *cosa-1 brc-1* mutants RAD-51 accumulation was dramatically prolonged until diplotene, whereas in the *brc-1; syp-2* mutant overall RAD-51 staining was dramatically reduced (Fig 6B, C). Aberrant chromosome structures occurred at a particularly high frequency in *brc-1; syp-2* mutants, consistent with the severe reduction in RAD-51 loading in pachytene nuclei (Fig 6A). Thus, in CO-defective mutants, BRC-1 regulation of RAD-51 dynamics is altered by the presence of the SC.

Efficient RAD-51-mediated repair upon exogenous DSB induction requires functional BRC-1

Exposure of *brc-1* and *brd-1* mutants to IR causes dose-dependent hypersensitivity which eventually culminates in full sterility, possibly due to the formation of highly unstructured chromatin bodies in diakinesis nuclei (46). These structures resemble those formed upon BRC-2/BRCA2 depletion, which in worms is essential for RAD-51 loading (31, 76), and COM-1/Sae2 depletion, which promotes DSB resection (68, 77). Both mutants lack RAD-51 recruitment onto DNA during meiotic prophase I. We therefore sought to investigate whether the aberrant chromatin masses observed in irradiated *brc-1* mutants were caused by impaired RAD-51 recruitment. To be efficiently loaded to the single-stranded DNA (ssDNA) tails generated after resection, RAD-51 must be exchanged with RPA (RPA-1 in worms), which

363 coats ssDNA tails to stabilize them and prevent DNA from self-winding (78, 79). We
364 generated a *brc-1* mutant strain expressing RPA-1::YFP (80) and analysed RAD-51 and
365 RPA-1 loading at two different time points post irradiation. We observed a dramatic
366 reduction in RAD-51 focus formation specifically in mid to late pachytene nuclei of *brc-1*
367 mutants, along with enhanced RPA-1 levels (Fig 7A). At 24 hours post irradiation, both
368 RAD-51 and RPA-1 were still abundant in *[rpa-1*::*YFP]* animals; in contrast, in *brc-1; [rpa-*
369 *1*::*YFP]* mutants RPA-1 was still expressed at higher levels than in controls, but RAD-51 was
370 remarkably reduced (Fig 7B). Prompted by these results, we decided to analyse the loading
371 dynamics of BRC-1::HA and RAD-51 after IR exposure to assess whether exogenous DSB
372 formation affects the mutual spatio-temporal regulation of these proteins. Under
373 physiological growth conditions, BRC-1 and RAD-51 localization did not overlap prior to
374 BRC-1 enrichment in the SC, which occurs after RAD-51 disappearance (Fig S6A, B). At
375 1 hour post irradiation, BRC-1::HA started to form discrete chromatin-associated foci in pre-
376 meiotic nuclei, often in close proximity to (but not co-localizing with) RAD-51 foci
377 (Fig S6A,B). Although abundant RAD-51 accumulation was triggered by IR exposure
378 throughout the germline, BRC-1::HA levels were only modestly increased. However, western
379 blot analysis revealed a shift in BRC-1::HA migration after IR which remained unchanged
380 throughout the time course (Fig S6C), suggesting that exogenous DNA damage might elicit
381 post-translational modifications of BRC-1. Western blot analysis also showed a slight
382 increase in BRC-1::HA abundance, confirming our immunofluorescence data (Fig S6A). In
383 meiotic nuclei, BRC-1 was detected along the SC at an earlier time point than in non-
384 irradiated animals, but retraction towards the short arms of bivalents appeared delayed
385 (Fig S6A). Samples analysed 8 hours after IR revealed robust BRC-1 and RAD-51 co-
386 localization in nuclei residing in the mitotic tip; however, as at the earlier time point, no clear
387 co-localization was observed in pachytene nuclei (Fig S6A, B). At 24 hours post irradiation,

388 BRC-1::HA foci in the mitotic nuclei had largely disappeared and bright RAD-51 foci were
389 observed only in enlarged, G2-arrested nuclei that were still undergoing repair; in contrast,
390 bright RAD-51 foci co-localizing with BRC-1 were occasionally seen in non-arrested nuclei.
391 Nuclei progressing through meiotic prophase I displayed more BRC-1 accumulation along
392 chromosomes at 24 hours post irradiation compared with unirradiated controls. Taken
393 together, our observations revealed that BRC-1 accumulation in the germline is modulated by
394 exogenous DNA damage and that the clear BRC-1 and RAD-51 co-localization observed
395 only in mitotic nuclei was cell cycle dependent.
396

397 ## Discussion

398 Our study sheds new light on the expression dynamics of the *C. elegans* BRC-1–BRD-1
399 heterodimer during meiotic prophase I and reveals that BRC-1 regulates RAD-51
400 accumulation in the germline under both unchallenged conditions and upon exogenous DNA
401 damage induction. We show that in contrast to mammalian meiosis, where BRCA1 is loaded
402 exclusively at asynapsed chromosome regions during spermatogenesis and oogenesis in
403 pachytene cells (52-54), in worms both BRC-1 and BRD-1 are expressed throughout meiotic
404 prophase I and are progressively enriched on the short arms of bivalents, in a CO- and SC-
405 dependent manner. Our data provide the first evidence that BRC-1 forms a complex in vivo
406 with the pro-CO factor MSH-5 and the SC central element SYP-3. Taken together, our
407 findings provide new insight into the meiotic functions of BRC-1 and BRD-1 and show that
408 the BCD complex is essential for preserving genome integrity and stimulating HR during
409 gametogenesis.
410

The BCD complex functions at the interface of synapsis and recombination

BRC-1 and BRD-1 display a highly dynamic localization pattern during meiotic prophase I progression, shifting from a pattern of rather diffuse accumulation at early stages to a robust association with the SC, which culminates in retention of the BCD complex at the region of the bivalent harbouring the chiasma (Figs 1–3). Remarkably, accumulation of BRC-1–BRD-1 at specific chromosomal subdomains occurred prior to retraction of the SC central elements to those domains but was concomitant with recombination factor-dependent enrichment of PLK-2 at the SC (Fig 2B) (63, 64), suggesting that the BCD complex is actively targeted to the region surrounding the CO rather than passively recruited following SC remodelling.

The fact that recruitment of BRC-1–BRD-1 to the region surrounding the chiasma has similar kinetics to PLK-2 recruitment and precedes SYP-1 redistribution suggests that the BCD complex (i) is brought into place via physical interaction with the CO machinery (Fig 3); (ii) might respond to changes in the physical properties of the SC, as triggered by chiasmata formation or (iii) might be directly induced by PLK-2.

Importantly, Li et al. (accompanying manuscript) observe the same localization pattern for BRC-1 and BRD-1 by employing GFP-tagged functional lines. However, in contrast with the aforementioned study in which they analysed localization in live worms, we did not detect BRD-1 loading in fixed *brc-1* mutant germlines, confirming what was previously reported in (50). This difference might be possibly due to distinctive processing of the samples or tag-dependent alterations of the properties of the fusion proteins (81).

Our data favour a model in which the SC is essential for initial recruitment of the BCD complex onto the chromosomes and later accumulates at the CO site due to the local concentration of recombination factors. In fact, BRC-1 recruitment to the SC is not prevented in *msh-5* or *spo-11* mutants (both of which are defective in CO formation but proficient in

436 synapsis establishment). However, similar to ZHP-3, BRC-1 fails to retract (Figs 3C and 4A).
437 Irradiation of *spo-11* mutants restored BRC-1 and ZHP-3 redistribution to the short arms of
438 bivalents (Fig 3D), confirming that CO establishment per se is the key trigger of local BCD
439 complex enrichment. Abrogation of synapsis dramatically changed the BRC-1 expression
440 pattern: it remained punctate throughout meiotic prophase I and displayed extensive and
441 specifically co-localization with RAD-51 in late pachytene cells (Fig 4B). However, in
442 mutants in which only one chromosome pair was asynapsed, such as *him-8* and *zim-2*
443 mutants, BRC-1 was not loaded onto the unsynapsed regions but loading dynamics were
444 normal for the other chromosome regions (Fig 4C, D). It was recently shown that PLK-2
445 plays a pivotal role in modulating the physical state of the SC in response to recombination
446 and that an absence of synapsis impairs PLK-2 redistribution from the nuclear envelope to
447 chromosome subdomains (63, 64, 82), which might explain the different BRC-1 localization
448 patterns in *syp-2* mutants. Different BRD-1 localization patterns were observed in *htp-1* and
449 *prom-1* mutants, but both were characterized by extensive non-homologous synapsis. BRD-1
450 accumulated in bright agglomerates in the nucleus, suggesting that SYP loading per se is not
451 sufficient to recruit BRC-1–BRD-1 onto the SC (Fig S6).
452

453 **Crosstalk between the BCD complex and RAD-51 is governed by the SC**
454 Blocking BRC-1 function had opposing effects on the progression of recombination
455 intermediates in *cosa-1* and *syp-2* (CO-defective) mutants. RAD-51 accumulation was
456 exacerbated in *cosa-1* single mutants and largely suppressed in *syp-2* mutants (Fig 6), leading
457 to the formation of aberrant chromatin masses in diakinesis nuclei both mutant backgrounds,
458 as previously reported (47). Based on genetic data, BRC-1 function was previously
459 postulated to be essential for IS repair of meiotic DSBs (47, 83, 84); our data corroborate this
460 model. In *cosa-1 brc-1* double mutants, the presence of an intact SC might still impose a

461 homologue-biased constraint for an inter-homologue, CO-independent pathway that relies on
462 RAD-51-mediated repair but not on BRC-1 function. However, in the absence of synapsis,
463 repair of recombination intermediates is probably channelled entirely through the IS repair
464 pathway because the sister chromatid is the only available repair template: SC depletion
465 triggers association of BRC-1 with RAD-51 in late pachytene cells at presumptive repair
466 sites, thereby promoting HR-mediated repair. We also observed fewer RAD-51 foci in *brc-1;*
467 *syp-2* double mutants during early pachytene, suggesting that BRC-1 is nonetheless required
468 to (directly or indirectly) promote efficient RAD-51 loading, although co-localization with
469 RAD-51 at meiotic onset might be very transient. We observed that a lack of BRC-1 reduces
470 the loading of recombination markers such as MSH-5 and RMH-1 in early pachytene,
471 suggesting that even in the presence of the SC, BRC-1–BRD-1 function is required to
472 efficiently promote the processing of recombination intermediates. Moreover, in *brc-1*
473 mutants exposed to exogenous DSB induction, RAD-51 is not efficiently retained in mid- to
474 late pachytene cells (Fig 7). This is not due to impaired resection, as shown by the abundant
475 recruitment of RPA-1, which stabilizes ssDNA. However, RAD-51 loading is comparable to
476 controls in later stages, suggesting that stabilization, rather than loading per se, might require
477 the action of the BCD complex. This is in line with the findings reported by Li et al. (see
478 accompanying manuscript).
479 When we scored BRC-1 levels after exposure to IR, we detected a slight increase in
480 abundance but a marked difference in protein migration on western blots (Fig S6), suggesting
481 that exogenous DNA damage promotes post-translational modification of BRC-1.
482 Importantly, despite dramatically enhanced RAD-51 levels upon irradiation, we observed
483 clear co-localization with BRC-1 only in mitotic cells and not during pachytene, once again
484 confirming that these proteins co-localize only when the SC is indeed absent (Fig S6).
485

Our findings suggest that the BCD complex responds to both synapsis and recombination and that the SC might act as a docking site for the BRC-1–BRD-1 complex to modulate its function in promoting DNA repair.

Materials and methods

Worm strains

All the worm strains used were grown at 20°C and the N2 Bristol strain was used as the wild type. The following alleles were used: LGI: *syp-3(ok758)*, *prom-1(ok1140)*; LGII: *[GFP*::*rmh-1]* (75), *[GFP*::*syp-3]* (67), *[GFP*::*cosa-1]* (20) ; LGIII: *brc-1(tm1145)*, *brc-1*::*HA* (this study), *brd-1(gk297)*, *cosa-1(tm3298)*, *OLLAS*::*cosa-1* (this study), *com-1(t1626);* LGIV: *spo-11(ok79)*, *him-8(tm611)*, *zim-2(tm574)*, *msh-5(me23)*, *GFP*::*msh-5* (this study), *htp-1(gk174)*, *rad-51(lg8701)*; LGV: *syp-2(ok307)*. No information is available on the chromosomal integration of *[rpa-1*::*YFP]* (80).

Cytological procedures

For cytological analysis of whole-mount gonads, age-matched worms (24 hours post-L4 stage) were dissected in 1× PBS on a Superfrost Plus charged slide and fixed with an equal volume of 2% PFA in 1× PBS for 5 min at room temperature. Slides were freeze-cracked in liquid nitrogen and then incubated in methanol -20°C for 5 min, followed by three washes in PBST (1× PBS, 0.1% Tween) at room temperature. Slides were blocked for 1 hour at room temperature in PBST containing 1% BSA and then primary antibodies were added in PBST and incubated overnight at 4°C. Slides were then washed in PBST at room temperature and secondary antibodies were applied for 2 hours. After three washes in PBST for 10 min each,

509 60 µl of a 2 µg/ml stock solution of DAPI in water was added to each slide and stained for
510 1 min at room temperature. Samples were washed again for at least 20 min in PBST and then
511 mounted with Vectashield. For detection of GFP::MSH-5, worms were dissected and fixed in
512 1× EGG buffer containing 0.1% Tween (instead of PBST). Detection of [RPA-1::YFP] was
513 performed as previously described (85). Primary antibodies used in this study were: mouse
514 monoclonal anti-HA tag (pre-absorbed on N2 worms to reduce non-specific binding; 1:1000
515 dilution; Covance), rabbit anti-HA tag (1:250 dilution; Invitrogen), rabbit anti-BRD-1 (1:500
516 dilution) (50), chicken anti-SYP-1 (1:400 dilution) (51), guinea pig anti-HTP-3 (1:500
517 dilution) (60), mouse monoclonal anti-GFP (1:500 dilution; Roche), guinea pig anti-ZHP-3
518 (1:500 dilution) (21), rabbit anti-OLLAS tag (pre-absorbed on N2 worms to reduce non-
519 specific binding; 1:1500 dilution; GenScript), rabbit anti-RAD-51 (1:10,000 dilution; SDIX)
520 and rabbit anti-PLK-2 (1:500 dilution) (86). Appropriate secondary antibodies were
521 conjugated with Alexa Fluor 488 or 594 (1:500 dilution) or with Alexa Fluor 647 (1:250
522 dilution). Images were collected as z-stacks (0.3 µm intervals) using an UPlanSApo 100x NA
523 1.40 objective on a DeltaVision System equipped with a CoolSNAP HQ2 camera. Files were
524 deconvolved with SoftWORx software and processed in Adobe Photoshop, where some false
525 colouring was applied. Samples acquired by super-resolution microscopy (Fig 3C) were
526 prepared as previously reported (63) without modifications and imaged with a DeltaVision
527 OMX.
528

529 **Biochemistry**

530 For whole-cell protein extraction, 200 age-matched animals (24 hours post-L4 stage) were
531 picked into 1× Tris-EDTA buffer (10 mM Tris pH 8, 1 mM EDTA) containing 1× protein
532 inhibitor cocktail (Roche), snap-frozen in liquid nitrogen. After thawing, an equal volume of

2× Laemmli buffer was added. Samples were boiled for 10 min, clarified and separated on pre-cast 4–20% gradient acrylamide gels (Bio Rad).

Fractionated protein extracts for western blotting and immunoprecipitation were prepared as previously reported (51). Western blotting used 50 µg protein samples from each fraction, whereas immunoprecipitation assays used at least 1 mg samples of pooled soluble nuclear and chromatin-bound fractions. Proteins were transferred onto nitrocellulose membrane for 1 hour at 4°C at 100V in 1× Tris-glycine buffer containing 20% methanol. Membranes were blocked for 1 hour in 1× TBS containing 0.1% Tween (TBST) and 5% milk; primary antibodies were added into the same buffer and incubated overnight at 4°C. Membranes were then washed in 1× TBST and then incubated with appropriate secondary antibodies in TBST containing 5% milk for 2 hours at room temperature. After washing, membranes were incubated with ECL and developed with a ChemiDoc system (BioRad). To detect phosphorylated CHK-1^{S345}, TBST containing 5% BSA (instead of milk) was used for blocking and antibody dilution. The following antibodies were used for western blotting: mouse monoclonal anti-HA tag (1:1000 dilution; Cell Signalling), rabbit anti-HA tag (1:500 dilution; Invitrogen), chicken anti-GFP (1:4000 dilution; Abcam), mouse anti-GAPDH (1:5000 dilution; Ambion), rabbit anti-Histone H3 (1:100,000 dilution; Abcam); rabbit anti-phospho-CHK-1^{S345} (1:1000 dilution; Cell Signalling), HRP-conjugated anti-mouse (1:2500 dilution) and anti-rabbit (1:25,000 dilution; both Jackson ImmunoResearch) and HRP-conjugated anti-chicken (1:10,000 dilution; Santa Cruz).

Irradiation

Age-matched worms (24 hours post-L4 stage) were exposed to the indicated dose of IR with a Gammacell irradiator containing a ^{137}Cs source. For viability screening, irradiated worms

were allowed to lay eggs for 24 hours and then removed; hatched versus unhatched eggs were scored the following day. For cytological analysis, worms were dissected and immunostained at the indicated times.

CRISPR-Cas9 Tagging

All the details relative to the tagging strategy followed to generate the *brc-1::HA*, *OLLAS::cosa-1* and *GFP::msh-5* lines are available upon request.

Acknowledgements

We are grateful to S. Boulton, N. Bhalla, E. Martinez-Perez, M. Zetka and R. Lin for kindly providing the anti-BRD-1, anti-ZHP-3, anti-SYP-1, anti-HTP-3 and anti-PLK-2 antibodies respectively. We thank A. Graf for performing the microinjections, and J. Yanowitz and J. Engebrecht for sharing unpublished data. Some strains were provided by the CGC, which is funded by the NIH Office of Research Infrastructure Programs (P40 OD010440). NS is the recipient of an Interdisciplinary Cancer Research fellowship (INDICAR) funded by the Mahlke-Obermann Stiftung and the European Union's Seventh Framework Programme for Research, Technological Development under grant agreement no 609431. Research in VJ laboratory is funded by the Austrian Science Fund (project no. SFB F3415-B19). MRDS was supported by the Austrian Science Fund doctoral programme (project no. W1238).

Author contributions

Conceptualization: NS.; Funding acquisition: NS.; Investigation: NS, EJ, MRDS.; Methodology: NS.; Project administration: NS.; Resources: NS VJ.; Visualization: NS. Writing (original draft): NS.

References

1. Zickler D. [The synaptonemal complex: a structure necessary for pairing, recombination or organization of the meiotic chromosome?]. J Soc Biol. 1999;193(1):17-22.
2. Zickler D, Kleckner N. Recombination, Pairing, and Synapsis of Homologs during Meiosis. Cold Spring Harb Perspect Biol. 2015;7(6).
3. Hillers KJ, Jantsch V, Martinez-Perez E, Yanowitz JL. Meiosis. WormBook. 2015:1-54.
4. Baudrimont A, Penkner A, Woglar A, Machacek T, Wegrostek C, Gloggnitzer J, et al. Leptotene/zygotene chromosome movement via the SUN/KASH protein bridge in Caenorhabditis elegans. PLoS Genet. 2010;6(11):e1001219.
5. Rosu S, Zawadzki KA, Stamper EL, Libuda DE, Reese AL, Dernburg AF, et al. The C. elegans DSB-2 protein reveals a regulatory network that controls competence for meiotic DSB formation and promotes crossover assurance. PLoS Genet. 2013;9(8):e1003674.
6. Stamper EL, Rodenbusch SE, Rosu S, Ahringer J, Villeneuve AM, Dernburg AF. Identification of DSB-1, a protein required for initiation of meiotic recombination in Caenorhabditis elegans, illuminates a crossover assurance checkpoint. PLoS Genet. 2013;9(8):e1003679.
7. Colaiacovo MP, MacQueen AJ, Martinez-Perez E, McDonald K, Adamo A, La Volpe A, et al. Synaptonemal complex assembly in C. elegans is dispensable for loading strand-exchange proteins but critical for proper completion of recombination. Dev Cell. 2003;5(3):463-74.
8. MacQueen AJ, Colaiacovo MP, McDonald K, Villeneuve AM. Synapsis-dependent and -independent mechanisms stabilize homolog pairing during meiotic prophase in C. elegans. Genes Dev. 2002;16(18):2428-42.
9. Cohen PE, Pollard JW. Regulation of meiotic recombination and prophase I progression in mammals. Bioessays. 2001;23(11):996-1009.
10. Zickler D, Kleckner N. Meiotic chromosomes: integrating structure and function. Annu Rev Genet. 1999;33:603-754.
11. Dernburg AF, McDonald K, Moulder G, Barstead R, Dresser M, Villeneuve AM. Meiotic recombination in C. elegans initiates by a conserved mechanism and is dispensable for homologous chromosome synapsis. Cell. 1998;94(3):387-98.
12. Keeney S, Neale MJ. Initiation of meiotic recombination by formation of DNA double-strand breaks: mechanism and regulation. Biochem Soc Trans. 2006;34(Pt 4):523-5.
13. Mets DG, Meyer BJ. Condensins regulate meiotic DNA break distribution, thus crossover frequency, by controlling chromosome structure. Cell. 2009;139(1):73-86.
14. Hillers KJ, Villeneuve AM. Chromosome-wide control of meiotic crossing over in C. elegans. Curr Biol. 2003;13(18):1641-7.
15. Zalevsky J, MacQueen AJ, Duffy JB, Kemphues KJ, Villeneuve AM. Crossing over during Caenorhabditis elegans meiosis requires a conserved MutS-based pathway that is partially dispensable in budding yeast. Genetics. 1999;153(3):1271-83.
16. Kelly KO, Dernburg AF, Stanfield GM, Villeneuve AM. Caenorhabditis elegans msh-5 is required for both normal and radiation-induced meiotic crossing over but not for completion of meiosis. Genetics. 2000;156(2):617-30.

17. Edelmann W, Cohen PE, Kneitz B, Winand N, Lia M, Heyer J, et al. Mammalian MutS homologue 5 is required for chromosome pairing in meiosis. Nat Genet. 1999;21(1):123-7.
18. Pochart P, Woltering D, Hollingsworth NM. Conserved properties between functionally distinct MutS homologs in yeast. J Biol Chem. 1997;272(48):30345-9.
19. Holloway JK, Sun X, Yokoo R, Villeneuve AM, Cohen PE. Mammalian CNTD1 is critical for meiotic crossover maturation and deselection of excess precrossover sites. J Cell Biol. 2014;205(5):633-41.
20. Yokoo R, Zawadzki KA, Nabeshima K, Drake M, Arur S, Villeneuve AM. COSA-1 reveals robust homeostasis and separable licensing and reinforcement steps governing meiotic crossovers. Cell. 2012;149(1):75-87.
21. Bhalla N, Wynne DJ, Jantsch V, Dernburg AF. ZHP-3 acts at crossovers to couple meiotic recombination with synaptonemal complex disassembly and bivalent formation in C. elegans. PLoS Genet. 2008;4(10):e1000235.
22. Jantsch V, Pasierbek P, Mueller MM, Schweizer D, Jantsch M, Loidl J. Targeted gene knockout reveals a role in meiotic recombination for ZHP-3, a Zip3-related protein in Caenorhabditis elegans. Mol Cell Biol. 2004;24(18):7998-8006.
23. Agarwal S, Roeder GS. Zip3 provides a link between recombination enzymes and synaptonemal complex proteins. Cell. 2000;102(2):245-55.
24. Rinaldo C, Bazzicalupo P, Ederle S, Hilliard M, La Volpe A. Roles for Caenorhabditis elegans rad-51 in meiosis and in resistance to ionizing radiation during development. Genetics. 2002;160(2):471-9.
25. Alpi A, Pasierbek P, Gartner A, Loidl J. Genetic and cytological characterization of the recombination protein RAD-51 in Caenorhabditis elegans. Chromosoma. 2003;112(1):6-16.
26. Martinez-Perez E, Villeneuve AM. HTP-1-dependent constraints coordinate homolog pairing and synapsis and promote chiasma formation during C. elegans meiosis. Genes Dev. 2005;19(22):2727-43.
27. Martinez-Perez E, Schvarzstein M, Barroso C, Lightfoot J, Dernburg AF, Villeneuve AM. Crossovers trigger a remodeling of meiotic chromosome axis composition that is linked to two-step loss of sister chromatid cohesion. Genes Dev. 2008;22(20):2886-901.
28. de Carvalho CE, Zaaijer S, Smolikov S, Gu Y, Schumacher JM, Colaiacovo MP. LAB-1 antagonizes the Aurora B kinase in C. elegans. Genes Dev. 2008;22(20):2869-85.
29. Clemons AM, Brockway HM, Yin Y, Kasinathan B, Butterfield YS, Jones SJ, et al. akirin is required for diakinesis bivalent structure and synaptonemal complex disassembly at meiotic prophase I. Mol Biol Cell. 2013;24(7):1053-67.
30. Zetka MC, Kawasaki I, Strome S, Muller F. Synapsis and chiasma formation in Caenorhabditis elegans require HIM-3, a meiotic chromosome core component that functions in chromosome segregation. Genes Dev. 1999;13(17):2258-70.
31. Martin JS, Winkelmann N, Petalcorin MI, McIlwraith MJ, Boulton SJ. RAD-51-dependent and -independent roles of a Caenorhabditis elegans BRCA2-related protein during DNA double-strand break repair. Mol Cell Biol. 2005;25(8):3127-39.
32. Prakash R, Zhang Y, Feng W, Jasin M. Homologous recombination and human health: the roles of BRCA1, BRCA2, and associated proteins. Cold Spring Harb Perspect Biol. 2015;7(4):a016600.
33. Schwertman P, Bekker-Jensen S, Mailand N. Regulation of DNA double-strand break repair by ubiquitin and ubiquitin-like modifiers. Nat Rev Mol Cell Biol. 2016;17(6):379-94.

677 34. Bachelier R, Xu X, Wang X, Li W, Naramura M, Gu H, et al. Normal lymphocyte
678 development and thymic lymphoma formation in Brca1 exon-11-deficient mice.
679 Oncogene. 2003;22(4):528-37.
680 35. Cao L, Li W, Kim S, Brodie SG, Deng CX. Senescence, aging, and malignant
681 transformation mediated by p53 in mice lacking the Brca1 full-length isoform. Genes
682 Dev. 2003;17(2):201-13.
683 36. Chandler J, Hohenstein P, Swing DA, Tessarollo L, Sharan SK. Human BRCA1 gene
684 rescues the embryonic lethality of Brca1 mutant mice. Genesis. 2001;29(2):72-7.
685 37. Cui J, Shen F, Jiang F, Wang Y, Bian J, Shen Z. [Loss of heterozygosity and
686 microsatellite instability in the region including BRCA1 of breast cancer in Chinese].
687 Zhonghua Yi Xue Yi Chuan Xue Za Zhi. 1998;15(6):348-50.
688 38. Gowen LC, Johnson BL, Latour AM, Sulik KK, Koller BH. Brca1 deficiency results
689 in early embryonic lethality characterized by neuroepithelial abnormalities. Nat Genet.
690 1996;12(2):191-4.
691 39. Hakem R, de la Pompa JL, Sirard C, Mo R, Woo M, Hakem A, et al. The tumor
692 suppressor gene Brca1 is required for embryonic cellular proliferation in the mouse.
693 Cell. 1996;85(7):1009-23.
694 40. Hohenstein P, Kielman MF, Breukel C, Bennett LM, Wiseman R, Krimpenfort P, et
695 al. A targeted mouse Brca1 mutation removing the last BRCT repeat results in apoptosis
696 and embryonic lethality at the headfold stage. Oncogene. 2001;20(20):2544-50.
697 41. Liu CY, Flesken-Nikitin A, Li S, Zeng Y, Lee WH. Inactivation of the mouse Brca1
698 gene leads to failure in the morphogenesis of the egg cylinder in early postimplantation
699 development. Genes Dev. 1996;10(14):1835-43.
700 42. Ludwig T, Chapman DL, Papaioannou VE, Efstratiadis A. Targeted mutations of
701 breast cancer susceptibility gene homologs in mice: lethal phenotypes of Brca1, Brca2,
702 Brca1/Brca2, Brca1/p53, and Brca2/p53 nullizygous embryos. Genes Dev.
703 1997;11(10):1226-41.
704 43. Ludwig T, Fisher P, Ganesan S, Efstratiadis A. Tumorigenesis in mice carrying a
705 truncating Brca1 mutation. Genes Dev. 2001;15(10):1188-93.
706 44. Shen SX, Weaver Z, Xu X, Li C, Weinstein M, Chen L, et al. A targeted disruption of
707 the murine Brca1 gene causes gamma-irradiation hypersensitivity and genetic
708 instability. Oncogene. 1998;17(24):3115-24.
709 45. Broering TJ, Alavattam KG, Sadreyev RI, Ichijima Y, Kato Y, Hasegawa K, et al.
710 BRCA1 establishes DNA damage signaling and pericentric heterochromatin of the X
711 chromosome in male meiosis. J Cell Biol. 2014;205(5):663-75.
712 46. Boulton SJ, Martin JS, Polanowska J, Hill DE, Gartner A, Vidal M. BRCA1/BARD1
713 orthologs required for DNA repair in Caenorhabditis elegans. Curr Biol. 2004;14(1):33-
714 9.
715 47. Adamo A, Montemauri P, Silva N, Ward JD, Boulton SJ, La Volpe A. BRC-1 acts in
716 the inter-sister pathway of meiotic double-strand break repair. EMBO Rep.
717 2008;9(3):287-92.
718 48. Paix A, Folkmann A, Rasoloson D, Seydoux G. High Efficiency, Homology-Directed
719 Genome Editing in Caenorhabditis elegans Using CRISPR-Cas9 Ribonucleoprotein
720 Complexes. Genetics. 2015;201(1):47-54.
721 49. Friedland AE, Tzur YB, Esvelt KM, Colaiacovo MP, Church GM, Calarco JA.
722 Heritable genome editing in C. elegans via a CRISPR-Cas9 system. Nat Methods.
723 2013;10(8):741-3.

50. Polanowska J, Martin JS, Garcia-Muse T, Petalcorin MI, Boulton SJ. A conserved pathway to activate BRCA1-dependent ubiquitylation at DNA damage sites. EMBO J. 2006;25(10):2178-88.
51. Silva N, Ferrandiz N, Barroso C, Tognetti S, Lightfoot J, Telecan O, et al. The fidelity of synaptonemal complex assembly is regulated by a signaling mechanism that controls early meiotic progression. Dev Cell. 2014;31(4):503-11.
52. Turner JM, Mahadevaiah SK, Fernandez-Capetillo O, Nussenzweig A, Xu X, Deng CX, et al. Silencing of unsynapsed meiotic chromosomes in the mouse. Nat Genet. 2005;37(1):41-7.
53. Turner JM, Aprelikova O, Xu X, Wang R, Kim S, Chandramouli GV, et al. BRCA1, histone H2AX phosphorylation, and male meiotic sex chromosome inactivation. Curr Biol. 2004;14(23):2135-42.
54. Scully R, Chen J, Plug A, Xiao Y, Weaver D, Feunteun J, et al. Association of BRCA1 with Rad51 in mitotic and meiotic cells. Cell. 1997;88(2):265-75.
55. Au WW, Henderson BR. The BRCA1 RING and BRCT domains cooperate in targeting BRCA1 to ionizing radiation-induced nuclear foci. J Biol Chem. 2005;280(8):6993-7001.
56. Fabbro M, Rodriguez JA, Baer R, Henderson BR. BARD1 induces BRCA1 intranuclear foci formation by increasing RING-dependent BRCA1 nuclear import and inhibiting BRCA1 nuclear export. J Biol Chem. 2002;277(24):21315-24.
57. Li M, Yu X. Function of BRCA1 in the DNA damage response is mediated by ADP-ribosylation. Cancer Cell. 2013;23(5):693-704.
58. Smolikov S, Eizinger A, Schild-Prufert K, Hurlburt A, McDonald K, Engebrecht J, et al. SYP-3 restricts synaptonemal complex assembly to bridge paired chromosome axes during meiosis in Caenorhabditis elegans. Genetics. 2007;176(4):2015-25.
59. Smolikov S, Schild-Prufert K, Colaiacovo MP. A yeast two-hybrid screen for SYP-3 interactors identifies SYP-4, a component required for synaptonemal complex assembly and chiasma formation in Caenorhabditis elegans meiosis. PLoS Genet. 2009;5(10):e1000669.
60. Goodyer W, Kaitna S, Couteau F, Ward JD, Boulton SJ, Zetka M. HTP-3 links DSB formation with homolog pairing and crossing over during C. elegans meiosis. Dev Cell. 2008;14(2):263-74.
61. Labella S, Woglar A, Jantsch V, Zetka M. Polo kinases establish links between meiotic chromosomes and cytoskeletal forces essential for homolog pairing. Dev Cell. 2011;21(5):948-58.
62. Harper NC, Rillo R, Jover-Gil S, Assaf ZJ, Bhalla N, Dernburg AF. Pairing centers recruit a Polo-like kinase to orchestrate meiotic chromosome dynamics in C. elegans. Dev Cell. 2011;21(5):934-47.
63. Pattabiraman D, Roelens B, Woglar A, Villeneuve AM. Meiotic recombination modulates the structure and dynamics of the synaptonemal complex during C. elegans meiosis. PLoS Genet. 2017;13(3):e1006670.
64. Machovina TS, Mainpal R, Daryabeigi A, McGovern O, Paouneskou D, Labella S, et al. A Surveillance System Ensures Crossover Formation in C. elegans. Curr Biol. 2016;26(21):2873-84.
65. Park SH, Cheong C, Idoyaga J, Kim JY, Choi JH, Do Y, et al. Generation and application of new rat monoclonal antibodies against synthetic FLAG and OLLAS tags for improved immunodetection. J Immunol Methods. 2008;331(1-2):27-38.

771 66. Idoyaga J, Cheong C, Suda K, Suda N, Kim JY, Lee H, et al. Cutting edge:
772 langerin/CD207 receptor on dendritic cells mediates efficient antigen presentation on
773 MHC I and II products in vivo. J Immunol. 2008;180(6):3647-50.
774 67. Rog O, Dernburg AF. Direct Visualization Reveals Kinetics of Meiotic
775 Chromosome Synapsis. Cell Rep. 2015.
776 68. Penkner A, Portik-Dobos Z, Tang L, Schnabel R, Novatchkova M, Jantsch V, et al. A
777 conserved function for a Caenorhabditis elegans Com1/Sae2/CtIP protein homolog in
778 meiotic recombination. EMBO J. 2007;26(24):5071-82.
779 69. Phillips CM, Dernburg AF. A family of zinc-finger proteins is required for
780 chromosome-specific pairing and synapsis during meiosis in C. elegans. Dev Cell.
781 2006;11(6):817-29.
782 70. Phillips CM, Wong C, Bhalla N, Carlton PM, Weiser P, Meneely PM, et al. HIM-8
783 binds to the X chromosome pairing center and mediates chromosome-specific meiotic
784 synapsis. Cell. 2005;123(6):1051-63.
785 71. Jantsch V, Tang L, Pasierbek P, Penkner A, Nayak S, Baudrimont A, et al.
786 Caenorhabditis elegans prom-1 is required for meiotic prophase progression and
787 homologous chromosome pairing. Mol Biol Cell. 2007;18(12):4911-20.
788 72. Yin J, Sobeck A, Xu C, Meetei AR, Hoatlin M, Li L, et al. BLAP75, an essential
789 component of Bloom's syndrome protein complexes that maintain genome integrity.
790 EMBO J. 2005;24(7):1465-76.
791 73. Raynard S, Bussen W, Sung P. A double Holliday junction dissolvasome
792 comprising BLM, topoisomerase IIIalpha, and BLAP75. J Biol Chem.
793 2006;281(20):13861-4.
794 74. Wu L, Bachrati CZ, Ou J, Xu C, Yin J, Chang M, et al. BLAP75/RMI1 promotes the
795 BLM-dependent dissolution of homologous recombination intermediates. Proc Natl
796 Acad Sci U S A. 2006;103(11):4068-73.
797 75. Jagut M, Hamminger P, Woglar A, Millonigg S, Paulin L, Mikl M, et al. Separable
798 Roles for a Caenorhabditis elegans RMI1 Homolog in Promoting and Antagonizing
799 Meiotic Crossovers Ensure Faithful Chromosome Inheritance. PLoS Biol.
800 2016;14(3):e1002412.
801 76. Petalcorin MI, Galkin VE, Yu X, Egelman EH, Boulton SJ. Stabilization of RAD-51-
802 DNA filaments via an interaction domain in Caenorhabditis elegans BRCA2. Proc Natl
803 Acad Sci U S A. 2007;104(20):8299-304.
804 77. Lemmens BB, Johnson NM, Tijsterman M. COM-1 promotes homologous
805 recombination during Caenorhabditis elegans meiosis by antagonizing Ku-mediated
806 non-homologous end joining. PLoS Genet. 2013;9(2):e1003276.
807 78. Chen R, Wold MS. Replication protein A: single-stranded DNA's first responder:
808 dynamic DNA-interactions allow replication protein A to direct single-strand DNA
809 intermediates into different pathways for synthesis or repair. Bioessays.
810 2014;36(12):1156-61.
811 79. Wold MS. Replication protein A: a heterotrimeric, single-stranded DNA-binding
812 protein required for eukaryotic DNA metabolism. Annu Rev Biochem. 1997;66:61-92.
813 80. Stergiou L, Eberhard R, Doukoumetzidis K, Hengartner MO. NER and HR
814 pathways act sequentially to promote UV-C-induced germ cell apoptosis in
815 Caenorhabditis elegans. Cell Death Differ. 2011;18(5):897-906.
816 81. Miyawaki A, Tsien RY. Monitoring protein conformations and interactions by
817 fluorescence resonance energy transfer between mutants of green fluorescent protein.
818 Methods Enzymol. 2000;327:472-500.

819 82. Nadarajan S, Lambert TJ, Altendorfer E, Gao J, Blower MD, Waters JC, et al. Polo-
820 like kinase-dependent phosphorylation of the synaptonemal complex protein SYP-4
821 regulates double-strand break formation through a negative feedback loop. Elife.
822 2017;6.
823 83. Wolters S, Ermolaeva MA, Bickel JS, Fingerhut JM, Khanikar J, Chan RC, et al. Loss
824 of Caenorhabditis elegans BRCA1 promotes genome stability during replication in smc-
825 5 mutants. Genetics. 2014;196(4):985-99.
826 84. Hong Y, Sonneville R, Agostinho A, Meier B, Wang B, Blow JJ, et al. The SMC-5/6
827 Complex and the HIM-6 (BLM) Helicase Synergistically Promote Meiotic Recombination
828 Intermediate Processing and Chromosome Maturation during Caenorhabditis elegans
829 Meiosis. PLoS Genet. 2016;12(3):e1005872.
830 85. Checchi PM, Lawrence KS, Van MV, Larson BJ, Engebrecht J. Pseudosynapsis and
831 decreased stringency of meiotic repair pathway choice on the hemizygous sex
832 chromosome of Caenorhabditis elegans males. Genetics. 2014;197(2):543-60.
833 86. Nishi Y, Rogers E, Robertson SM, Lin R. Polo kinases regulate C. elegans
834 embryonic polarity via binding to DYRK2-primed MEX-5 and MEX-6. Development.
835 2008;135(4):687-97.
836

837

Figure captions

Fig 1. BRC-1–BRD-1 expression and localization during gametogenesis. (A) BRC-1::HA function was assessed by exposing worms to IR and then scoring the hatch rate of embryos laid in the following 24 hours. The mean of two independent experiments is shown. (B) Left: western blot analysis using an anti-HA antibody to monitor BRC-1::HA expression in whole-cell extracts. Actin was the loading control. Right: protein fractionation showing BRC-1::HA enrichment in the nucleus. Equal amounts of protein were loaded for each fraction. C = cytosol, NS = soluble nuclear pool, CB= chromatin-bound pool. GAPDH and histone H3 were used as loading controls for the cytosolic and chromatin-bound samples, respectively. (C) Top: whole-mount gonad from *brc-1*::*HA* worms dissected and stained with DAPI and anti-HA antibody, showing ubiquitous BRC-::HA expression throughout the germline. Note the progressive enrichment on the SC and short arms of bivalents. Bottom: enlarged images of specific regions of the gonad: mitotic tip (red frame), mid-pachytene (yellow frame) and late pachytene/diplotene (magenta frame). Scale bar, 10 μm. (D) Late pachytene nuclei stained with DAPI and anti-HA and BRD-1 antibodies display full co-localization of BRC-1::HA and BRD-1. Scale bar, 10 μm.

Fig 2. BRC-1 is enriched on the short arms of bivalents and co-localizes with SYP-1 and PLK-2. (A) BRC-1::HA, HTP-3 and SYP-1 localization patterns at different stages of meiotic prophase I. TZ = transition zone, MP = mid-pachytene, LP = late pachytene, DP = diplotene. Scale bar, 5 μm. (B) BRC-1::HA co-staining with anti-PLK-2 and anti-SYP-1 shows that BRC-1 is recruited concomitantly with PLK-2 and before SYP-1 to the shorts arm of bivalents. Scale bar, 30 μm (left) and 5 μm (right).

Fig 3. BRC-1 forms a complex with the CO machinery and the SC in vivo. (A) BRC-1::HA co-localizes with pro-CO factor COSA-1 in late prophase I. MP/LP = mid-/late pachytene, LP/DP = late pachytene/diplotene. Scale bar, 5 μm. (B) BRC-1::HA co-localizes with ZHP-3 and GFP::MSH-5 in late pachytene nuclei. Scale bar, 5 μm. (C) Partial projections of nuclei under super-resolution structured illumination microscopy: different examples show BRC-1::HA localization in the region surrounding the COSA-1-labelled CO site. BRC-1::HA forms a nodule-like structure together with SYP-1. (D) Late pachytene nuclei in non-irradiated samples show altered BRC-1::HA localization in *spo-11* mutants: BRC-1 and ZHP-3 remain localized along the SC without retraction to the short arms of bivalents. (E) Ionizing radiation rescues ZHP-3 and BRC-1::HA redistribution in *spo-11* mutants. (F) BRC-1::HA co-immunoprecipitates with GFP::MSH-5 and GFP::SYP-3 in vivo. GFP pull-downs were also performed in wild-type worms (WT) as a negative control.

Fig 4. Recombination and synapsis differentially regulate BRC-1 localization. (A) BRC-1::HA localization was assessed in *msh-5* and *rad-51* mutants. In the *msh-5* mutant, BRC-1::HA accumulates in the SC, as in *spo-11* mutants; in the *rad-51* mutant, it displays interspersed staining, and association with the SC is strongly reduced. Scale bar, 10 μm. (B) Abrogation of synapsis triggers BRC-1::HA accumulation into discrete chromatin-associated foci which co-localize with RAD-51 in late pachytene cells. Scale bar, 5 μm. (C) Unlike in the *him-8* or *zim-2* mutant, respectively, BRC-1::HA does not accumulate on asynapsed chromosome X or V in late pachytene nuclei. Arrows indicate regions of DNA devoid of both SYP-1 and BRC-1::HA. Scale bar, 5 μm. (D) Diplotene nuclei of *him-8* and *zim-2* mutants clearly lack BRC-1::HA on asynapsed univalents (circled). Scale bar, 5 μm.

887 **Fig 5. Analysis of recombination markers in *brc-1* mutants.** (A) Quantification of
888 GFP::RMH1, GFP::MSH-5 and OLLAS::COSA-1 markers in *brc-1* mutants and control
889 animals. Gonads were divided into four equal regions from the transition zone to the late
890 pachytene stage. The average number of foci per nucleus from at least three gonads per
891 genotype is shown. For GFP::RMH-1 and OLLAS::COSA-1 quantification, the number of
892 nuclei scored for each gonad region in the controls (and *brc-1* mutants) were: zone 1, 242
893 (334); zone 2, 185 (244); zone 3, (181 (214); zone 4, 124 (136). For GFP::MSH-5
894 quantification, the equivalent numbers were: zone 1, 230 (403); zone 2, 210 (410); zone 3,
895 165 (303); zone 4, 121 (147). Error bars show S.E.M. (B) Representative nuclei at different
896 meiotic stages co-stained for GFP::RMH-1 with OLLAS::COSA-1 (upper panels) or
897 GFP::MSH-5 (lower panels). Scale bar, 5 μm. Note that both GFP::RMH-1 and GFP::MSH-5
898 are expressed in fewer foci in early and mid-pachytene but not in late pachytene in *brc-1*
899 mutants.
900
901 **Fig 6. Loss of BRC-1 differently influences RAD-51 loading in *cosa-1* and *syp-2***
902 **mutants.** (A) Left: quantification of DAPI-stained bodies in diakinesis nuclei in different
903 genotypes. Number of diakinesis nuclei scored: *cosa-1*, 42; *cosa-1 brc-1*, 48; *syp-2*, 31; *brc-*
904 *1; syp-2*, 79. Right: representative images of DAPI-stained diakinesis nuclei. Scale bar, 3 μm.
905 (B) Quantification of RAD-51 foci per nucleus throughout the germline. Each gonad was
906 divided into seven equal zones and RAD-51 foci were counted in each nucleus. Data show
907 the average of at least three gonads for each genotype. Number of nuclei scored from zone 1
908 to zone 7 in different mutants: *cosa-1* – 162, 225, 179, 165, 142, 107, 124; *cosa-1 brc-1* –
909 347, 335, 285, 274, 228, 175, 149; *syp-2* – 244, 265, 241, 233, 190, 131, 118; *brc-1; syp-2* –
910 226, 305, 275, 297, 254, 161, 147. Error bars show S.E.M. (C) Whole-mount gonad stained
911 with DAPI and anti-RAD-51 antibody. Note accumulation of RAD-51 foci in late pachytene

912 in *cosa-1 brc-1* double mutants, which is not observed in *cosa-1* single mutants. In *brc-1;*
913 *syp-2* animals, the number of RAD-51 foci was dramatically reduced. Scale bars, 30 μm.
914
915 **Fig 7. Efficient accumulation/exchange of RAD-51 and RPA-1 upon exogenous DNA**
916 **damage requires BRC-1 function.** (A) Time course analysis of RAD-51 and RPA-1::YFP
917 DNA loading in irradiated *brc-1* and controls. Worms were irradiated with 75 Gy IR and
918 analysed after 8 hours. Nuclei in mid-pachytene display enhanced RPA-1 levels and
919 drastically reduced RAD-51 levels in *brc-1* mutants compared with controls. (B) The same
920 analysis performed at 24 hours post irradiation showed severely reduced RAD-51, with
921 higher RPA-1 levels that were identical to those at the earlier time point. Scale bars, 30 μm.

922 ## Supplementary figure captions

923
924 **S1 Fig. BRD-1 and BRC-1 localization patterns are identical during meiotic prophase I.**
925 (A) BRD-1 and SYP-1 immunostaining in wild-type animals shows that the BRD-1
926 expression pattern is identical to the one observed for BRC-1::HA. Note enrichment on the
927 SC and retraction to the short arms of bivalents. Scale bar, 30 μm. (B) Interdependent DNA
928 loading for BRD-1 and BRC-1 is shown by a lack of DNA-binding by BRD-1 in *brc-1*
929 mutant germlines. Scale bar, 5 μm.
930
931 **S2 Fig. BRD-1 is enriched at chromosome subdomains containing presumptive CO**
932 **sites.** Late pachytene nuclei of *[GFP*::*cosa-1]* animals were stained for BRD-1, GFP and
933 SYP-1. As previously observed for BRC-1, BRD-1 is progressively enriched at regions
934 surrounding the CO site. Scale bar, 5 μm.
935

936 **S3 Fig. Association of BRD-1 with the SC is largely disrupted in DSBs resection-**
937 **defective *com-1* mutants.** Mid-/late pachytene nuclei of the wild type (WT) and *com-1*
938 mutant were stained for BRD-1. BRD-1 loading onto the SC is drastically reduced when
939 DNA resection is impaired. Scale bar, 5 μm.
940
941 **S4 Fig. Non-homologous synapsis largely impairs loading of BRD-1, leading to**
942 **nucleoplasmic accumulation.** Late pachytene nuclei in the wild-type (WT) and *htp-1* and
943 *prom-1* mutants were stained with BRD-1, SYP-1 and HTP-3. In both mutants, BRD-1 is
944 largely excluded from the SC and forms nucleoplasmic agglomerates. Scale bar, 5 μm.
945
946 **S5 Fig. Synapsis and chiasmata formation occur normally but RAD-51 foci accumulate**
947 **in the *brc-1* mutant.** (A) SC assembly in the wild type (WT) and *brc-1* mutant was
948 monitored by co-staining for the axial element HTP-3 and central element SYP-1. The *brc-1*
949 mutant had no obvious defect in establishing synapsis. Scale bar, 5 μm. (B) DAPI-staining of
950 diakinesis nuclei does not show defective chiasmata formation in the *brc-1* mutant. Scale bar,
951 5 μm. Number of diakinesis nuclei analysed: WT, 44; *brc-1* mutant, 46. Error bars show
952 standard deviation. (C) Top: quantification revealed an accumulation and delayed
953 disappearance of RAD-51 foci in the absence of BRC-1. Bottom: representative nuclei from
954 early pachytene (EP) and late pachytene (LP) stages stained with DAPI and anti-RAD-51
955 antibody. Scale bar, 5 μm. For RAD-51 foci quantification, the following numbers of nuclei
956 were counted in each region in WT (and the *brc-1* mutant): zone 1, 154 (173); zone 2, 226
957 (189); zone 3, 189 (186); zone 4, 157 (156); zone 5, 113 (136); zone 6, 95 (125); zone 7, 92
958 (72). Error bars show S.E.M.
959

960 **S6 Fig. Exogenous DNA damage increases BRC-1 levels and triggers its association with**
961 **RAD-51 in mitotic nuclei.** (A) Whole-mount gonads of irradiated and non-irradiated *brc-*
962 *1*::*HA* worms immunostained for HA and RAD-51. Animals were exposed 75 Gy IR and
963 analysed at the indicated time points. (B) Representative nuclei from the pre-meiotic region
964 (MT) and late pachytene (LP) stage of gonads analysed at different times after IR. Note
965 BRC-1::HA focus formation in pre-meiotic nuclei, along with robust co-localization with
966 RAD-51 at 8 hours and occasionally at 24 hours post irradiation. Scale bars, 5 μm. (C)
967 Western blot analysis of whole-cell extracts show a shift in BRC-1::HA migration after
968 irradiation. Wild-type (wt) worms were the negative control. Actin was the loading control
969 and induction of phosphorylated CHK-1^{Ser345} was used as a positive control for irradiation.
970 The ratio of BRC-1::HA to actin (HA/Actin) is shown as an abundance index.
971

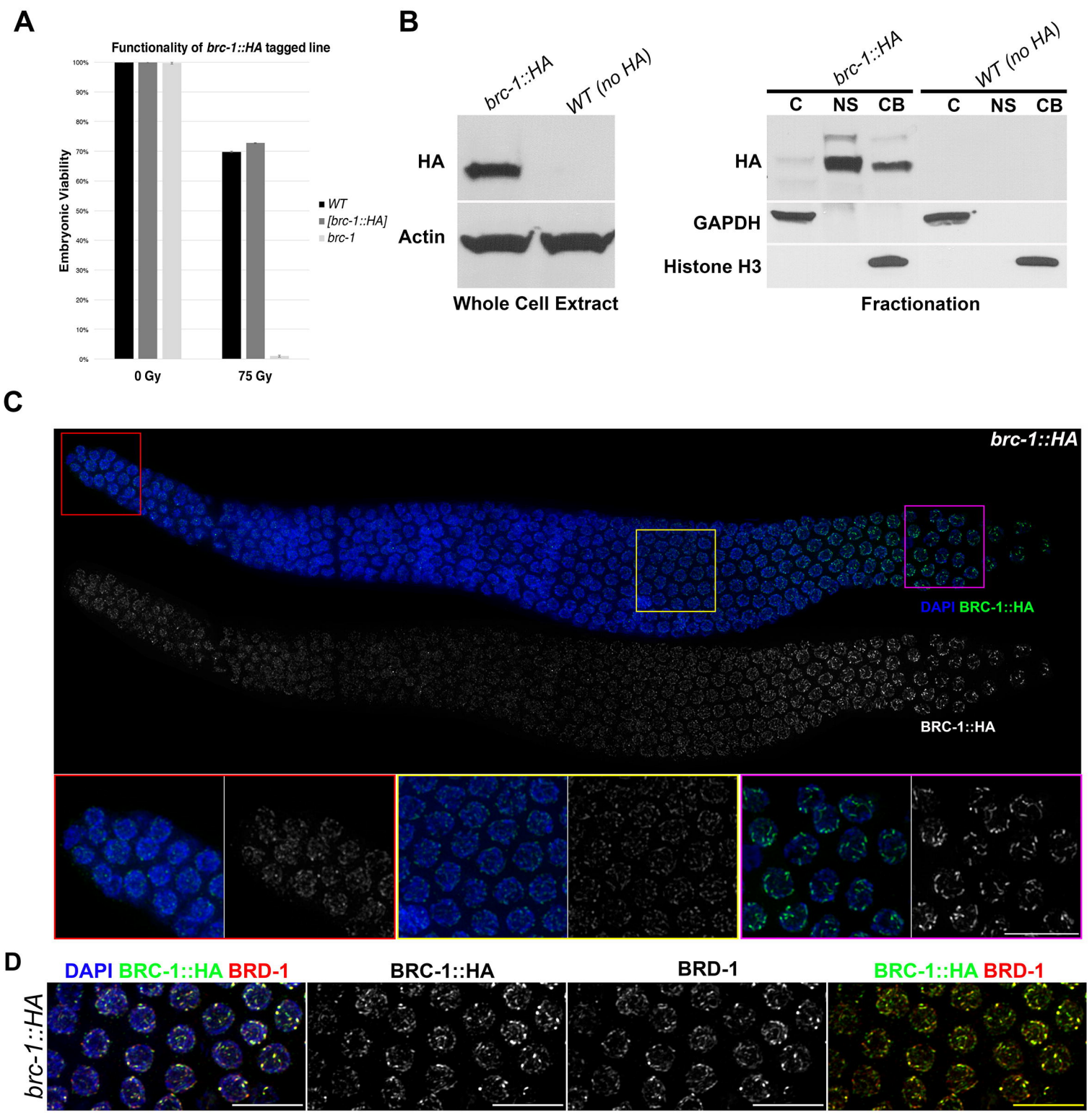
A
Functionality of brc-1::HA tagged line
Embryonic Viability
100%
90%
80%
70%
60%
50%
40%
30%
20%
10%
0%
0 Gy
75 Gy
WT
[brc-1::HA]
brc-1
B
brc-1::HA
WT (no HA)
HA
Actin
Whole Cell Extract
brc-1::HA
WT (no HA)
C
NS
CB
C
NS
CB
HA
GAPDH
Histone H3
Fractionation
C
brc-1::HA
DAPI BRC-1::HA
BRC-1::HA
D
DAPI BRC-1::HA BRD-1
BRC-1::HA
BRD-1
BRC-1::HA BRD-1
brc-1::HA

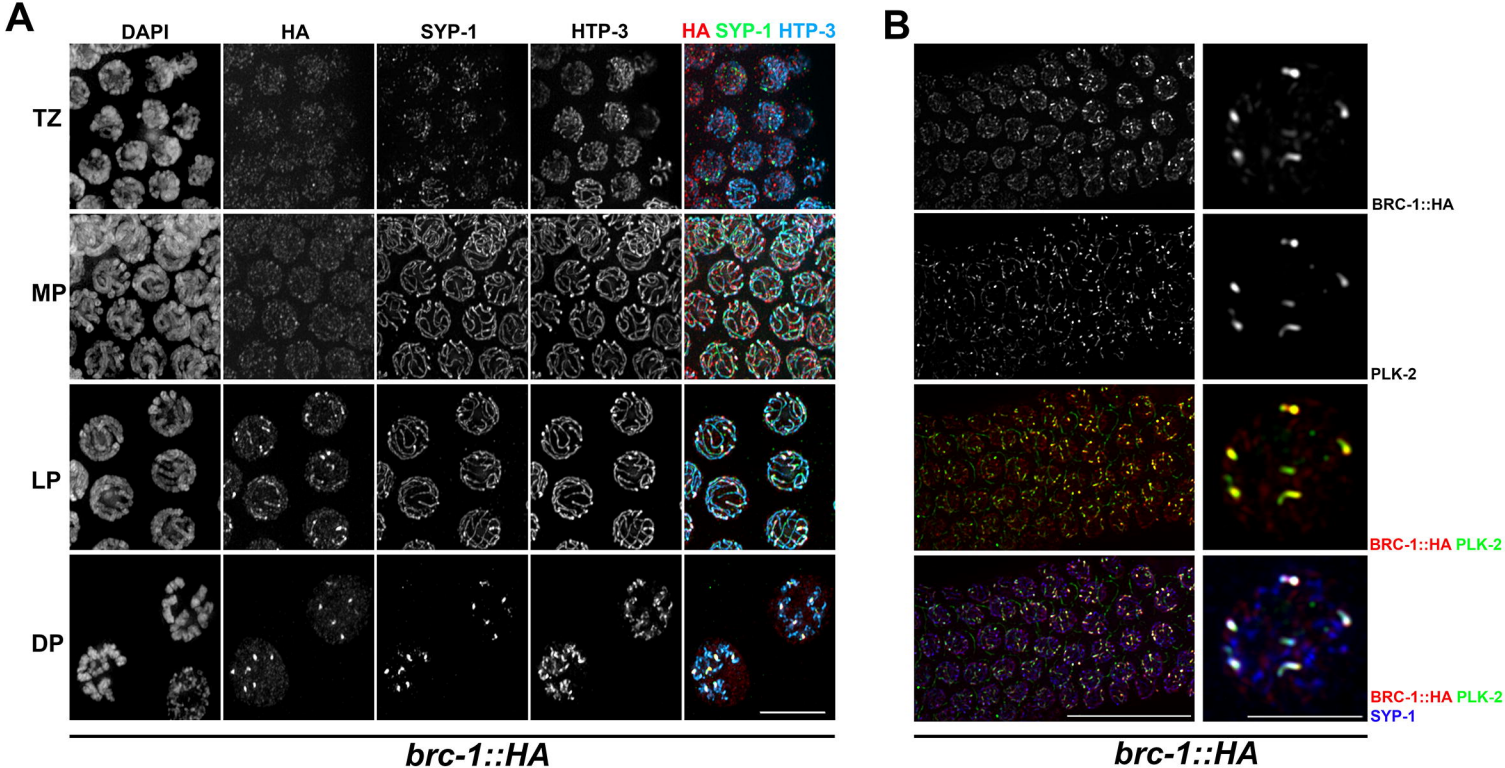
A
DAPI
HA
SYP-1
HTP-3
HA SYP-1 HTP-3
TZ
MP
LP
DP
brc-1::HA
B
BRC-1::HA
PLK-2
BRC-1::HA PLK-2
BRC-1::HA PLK-2
SYP-1
brc-1::HA

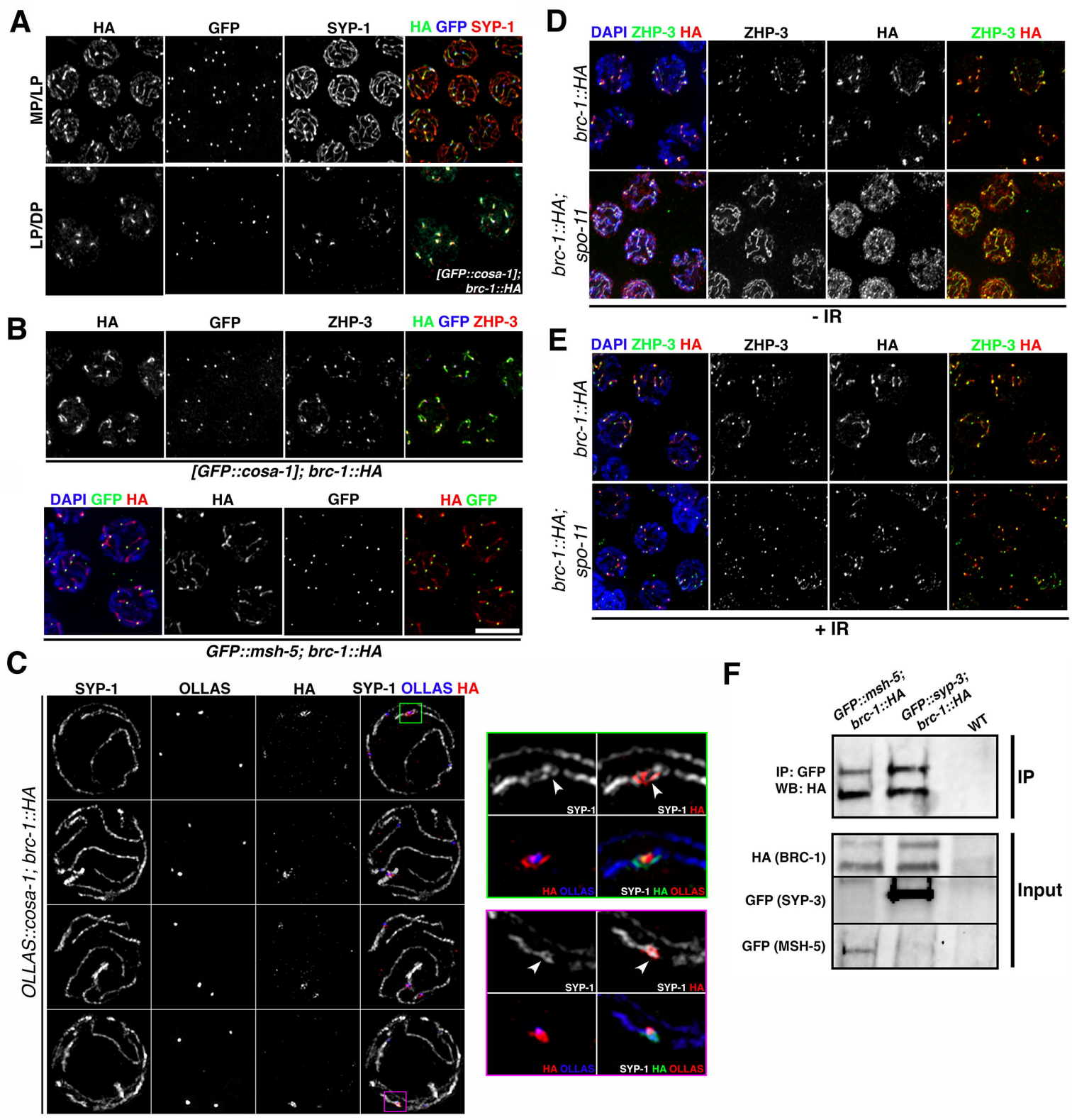
A
HA
GFP
SYP-1
HA GFP SYP-1
MP/LP
LP/DP
[GFP::cosa-1];
brc-1::HA
B
HA
GFP
ZHP-3
HA GFP ZHP-3
[GFP::cosa-1]; brc-1::HA
DAPI GFP HA
HA
GFP
HA GFP
GFP::msh-5; brc-1::HA
C
SYP-1
OLLAS
HA
SYP-1 OLLAS HA
OLLAS::cosa-1; brc-1::HA
SYP-1
SYP-1 HA
HA OLLAS
SYP-1 HA OLLAS
SYP-1
SYP-1 HA
HA OLLAS
SYP-1 HA OLLAS
D
DAPI ZHP-3 HA
ZHP-3
HA
ZHP-3 HA
brc-1::HA
brc-1::HA; spo-11
- IR
E
DAPI ZHP-3 HA
ZHP-3
HA
ZHP-3 HA
brc-1::HA
brc-1::HA; spo-11
+ IR
F
GFP::msh-5; brc-1::HA
GFP::syp-3; brc-1::HA
WT
IP: GFP
WB: HA
IP
HA (BRC-1)
GFP (SYP-3)
GFP (MSH-5)
Input

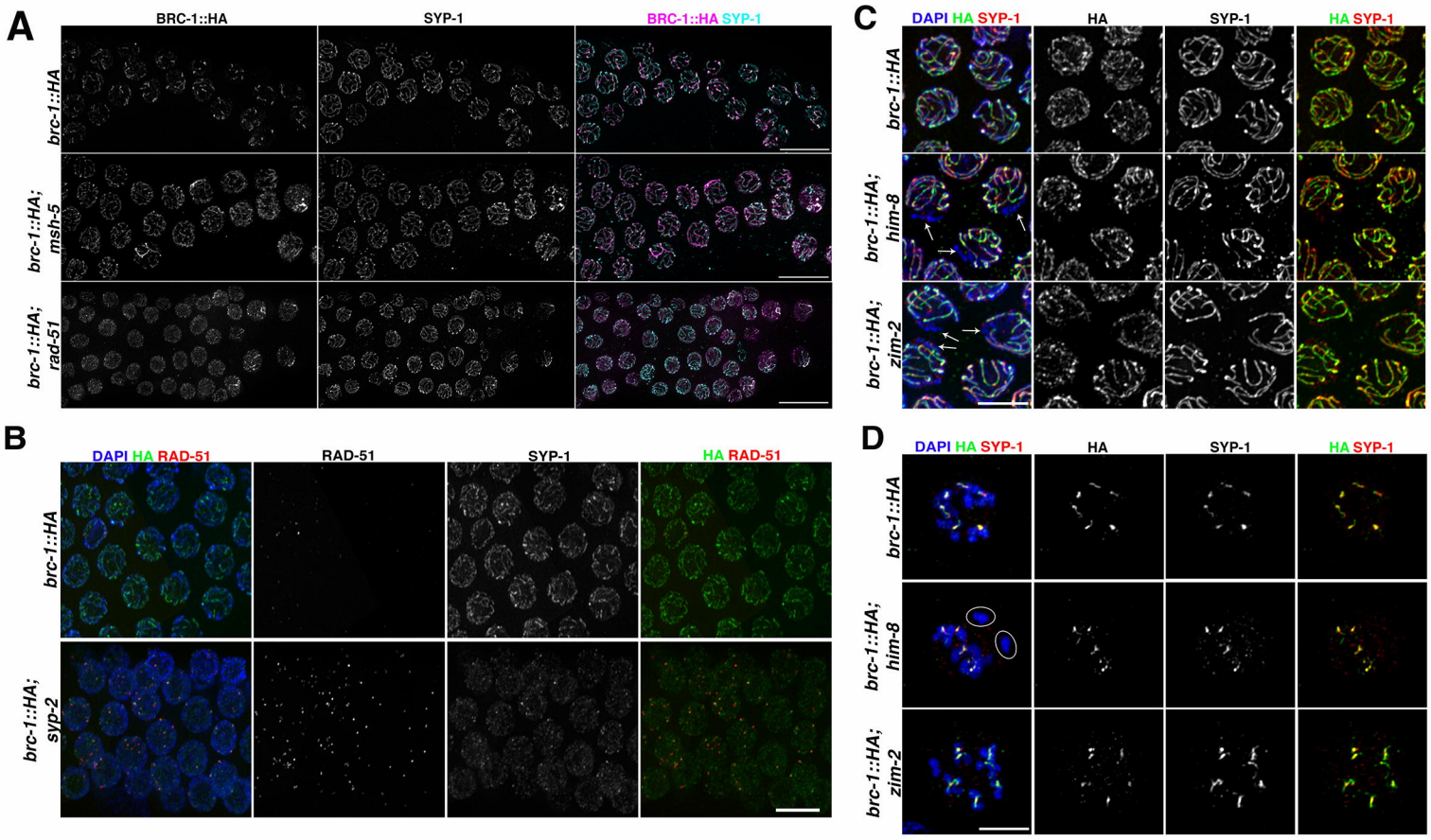
A
BRC-1::HA
SYP-1
BRC-1::HA SYP-1
brc-1::HA
brc-1::HA; msh-5
brc-1::HA; rad-51
B
DAPI HA RAD-51
RAD-51
SYP-1
HA RAD-51
brc-1::HA
brc-1::HA; syp-2
C
DAPI HA SYP-1
HA
SYP-1
HA SYP-1
brc-1::HA
brc-1::HA; him-8
brc-1::HA; zim-2
D
DAPI HA SYP-1
HA
SYP-1
HA SYP-1
brc-1::HA
brc-1::HA; him-8
brc-1::HA; zim-2

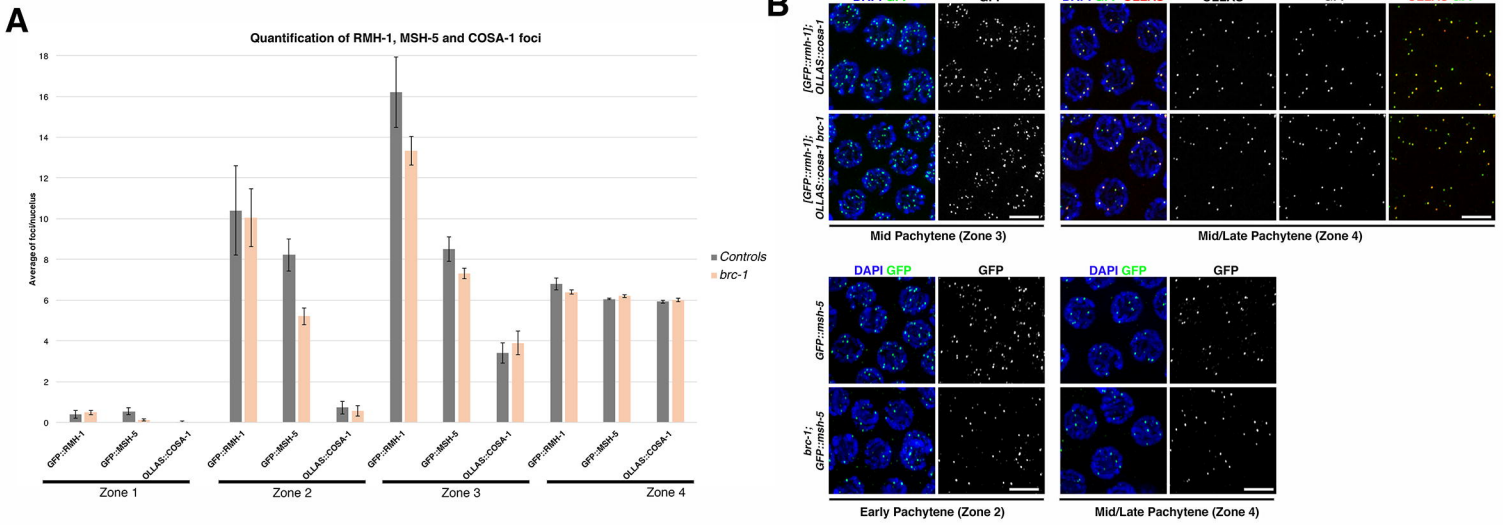
A
Quantification of RMH-1, MSH-5 and COSA-1 foci
Average of foci/nucleus
18
16
14
12
10
8
6
4
2
0
Controls
brc-1
GFP::RMH-1
GFP::MSH-5
OLLAS::COSA-1
Zone 1
Zone 2
Zone 3
Zone 4
B
DAPI GFP
GFP
DAPI GFP OLLAS
OLLAS
OLLAS GFP
[GFP::rmh-1]; OLLAS::cosa-1
[GFP::rmh-1]; OLLAS::cosa-1 brc-1
Mid Pachytene (Zone 3)
Mid/Late Pachytene (Zone 4)
GFP::msh-5
brc-1; GFP::msh-5
Early Pachytene (Zone 2)
Mid/Late Pachytene (Zone 4)

A

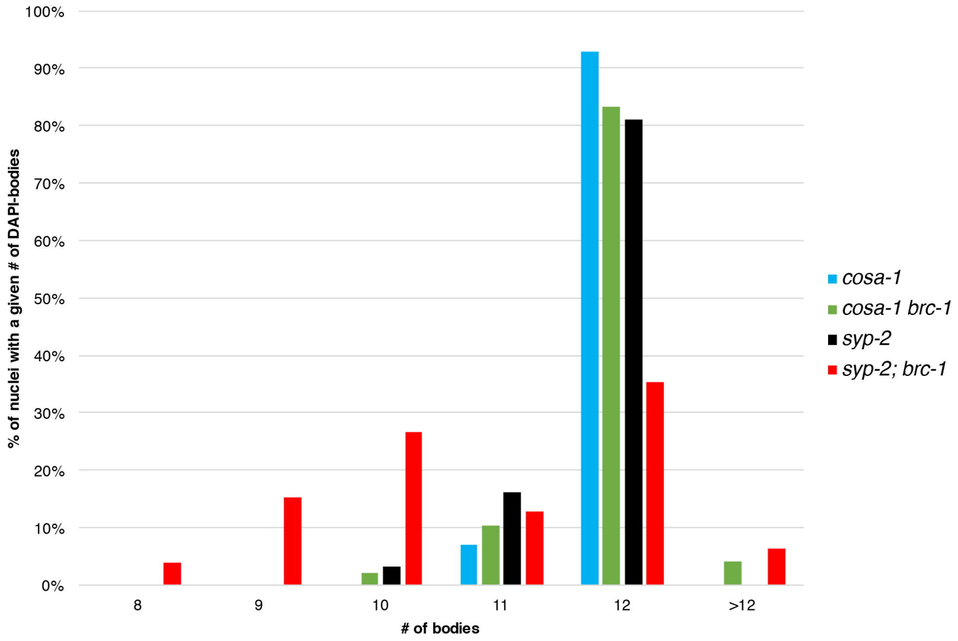

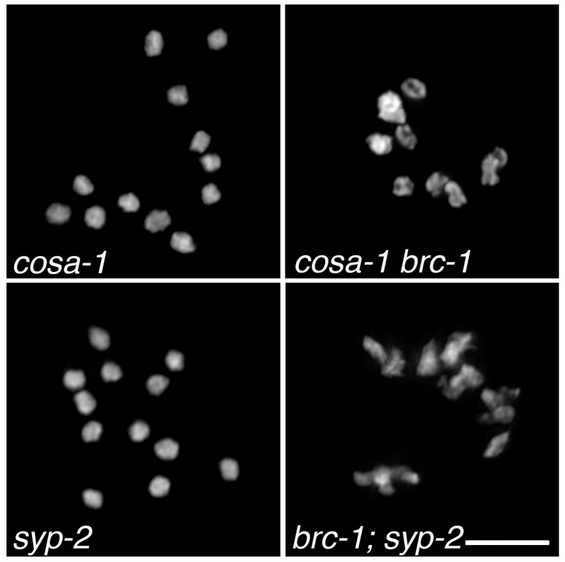

B

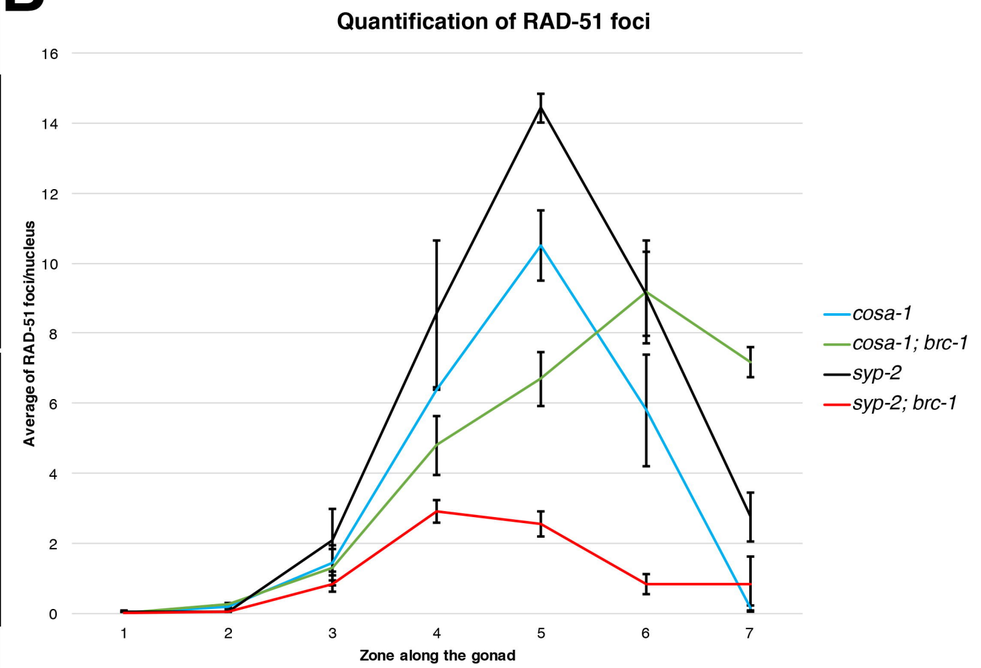

C

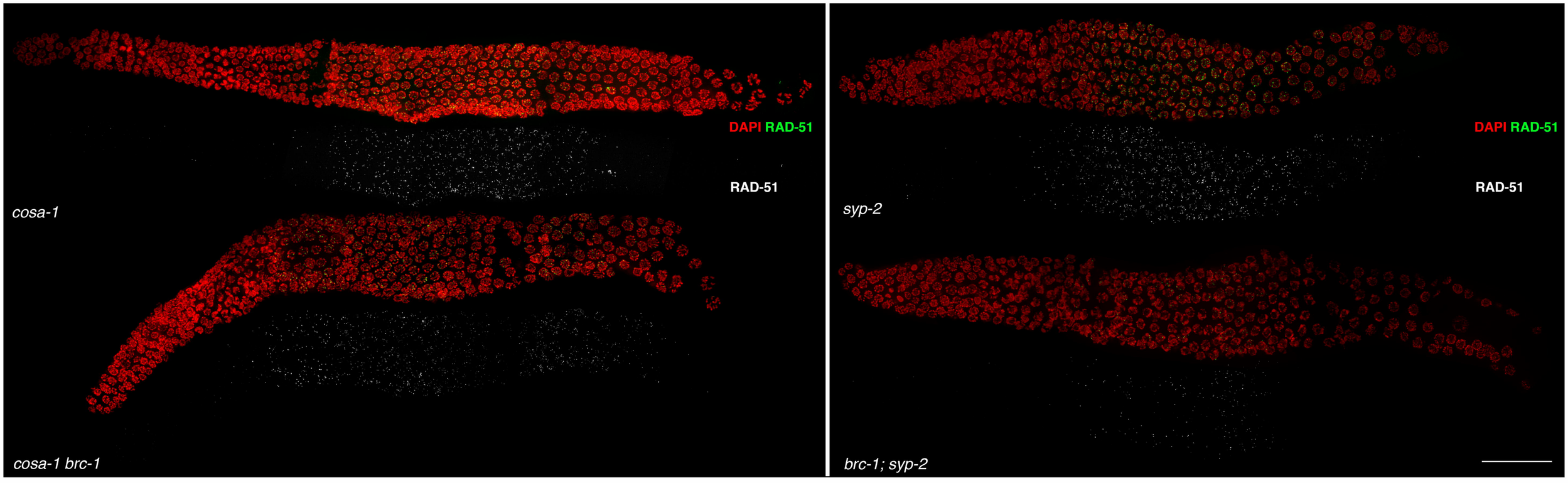

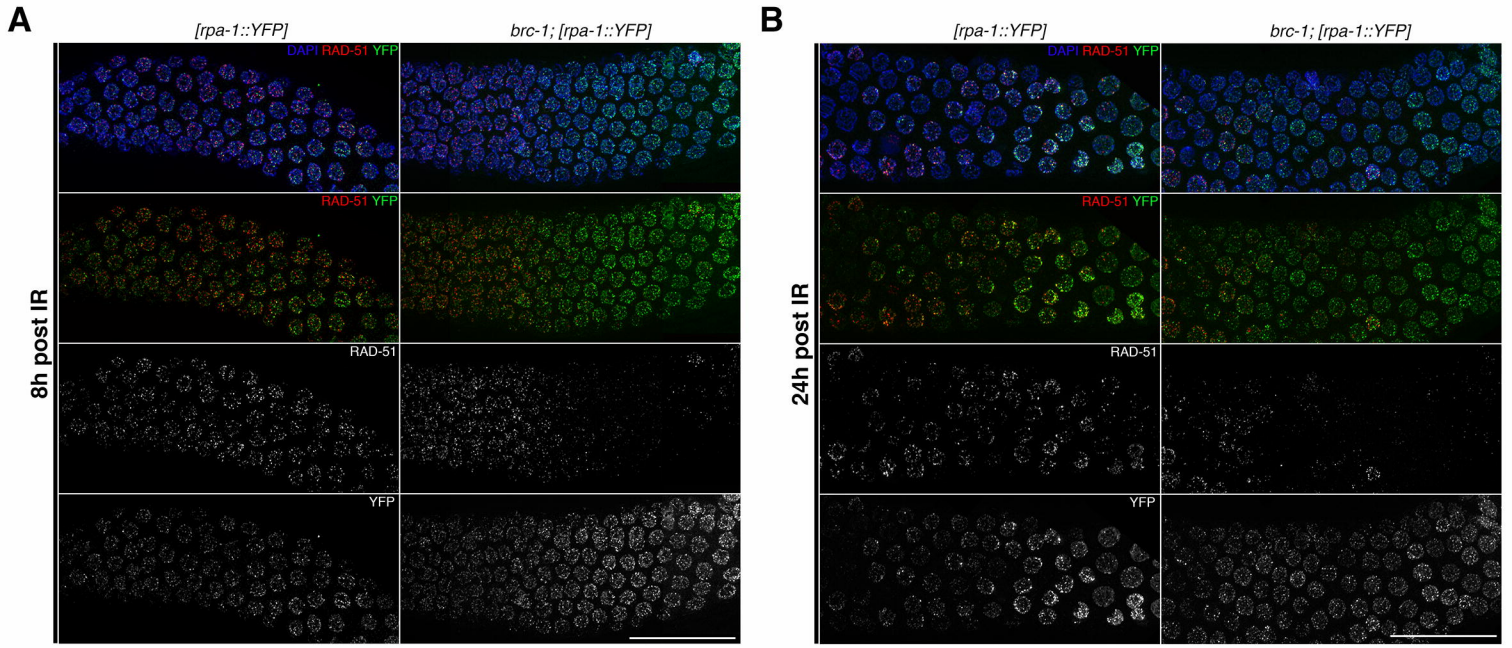
A
[rpa-1::YFP]
brc-1; [rpa-1::YFP]
8h post IR
DAPI RAD-51 YFP
RAD-51 YFP
RAD-51
YFP
B
[rpa-1::YFP]
brc-1; [rpa-1::YFP]
24h post IR
DAPI RAD-51 YFP
RAD-51 YFP
RAD-51
YFP

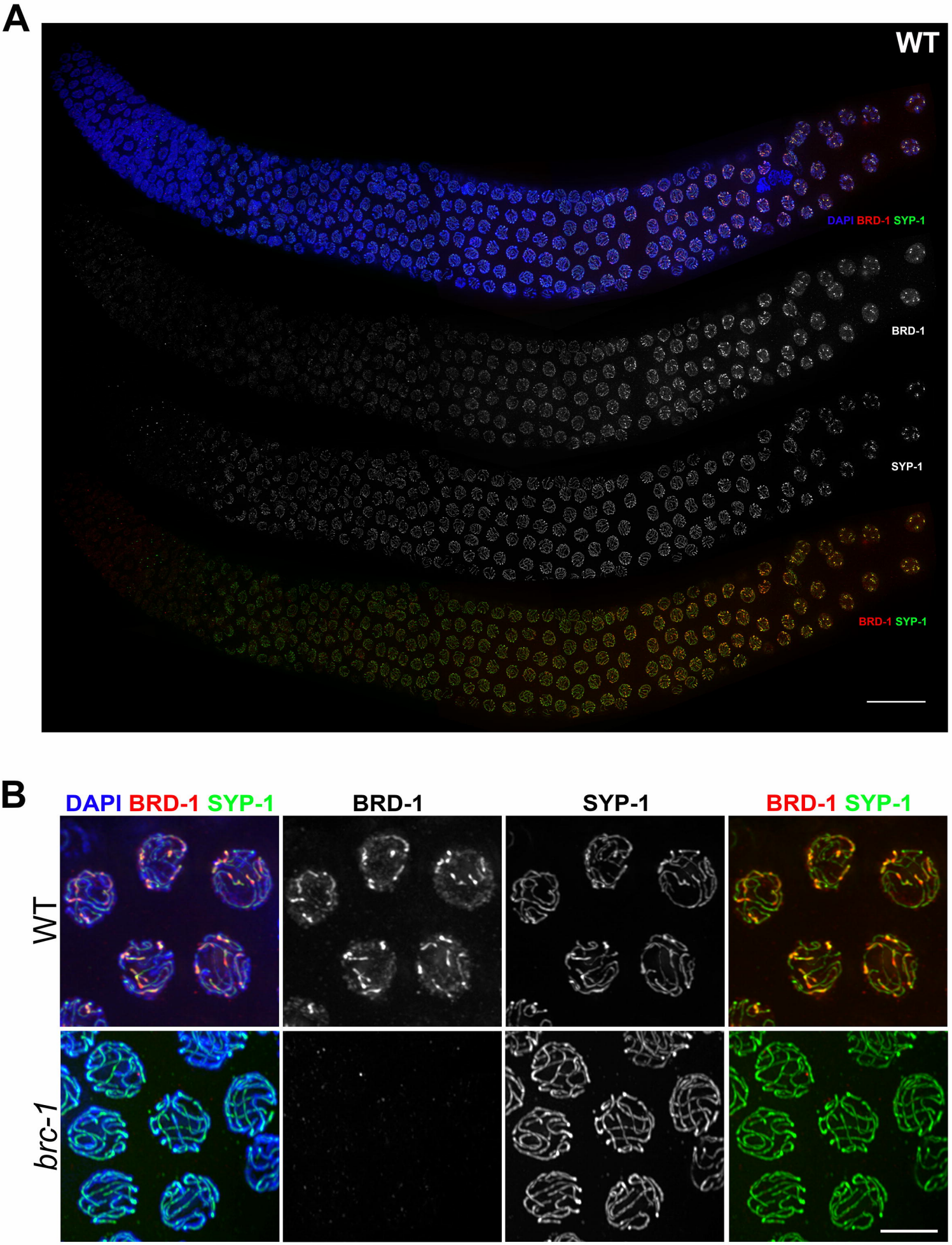
A
WT
DAPI BRD-1 SYP-1
BRD-1
SYP-1
BRD-1 SYP-1
B
DAPI BRD-1 SYP-1
BRD-1
SYP-1
BRD-1 SYP-1
WT
brc-1

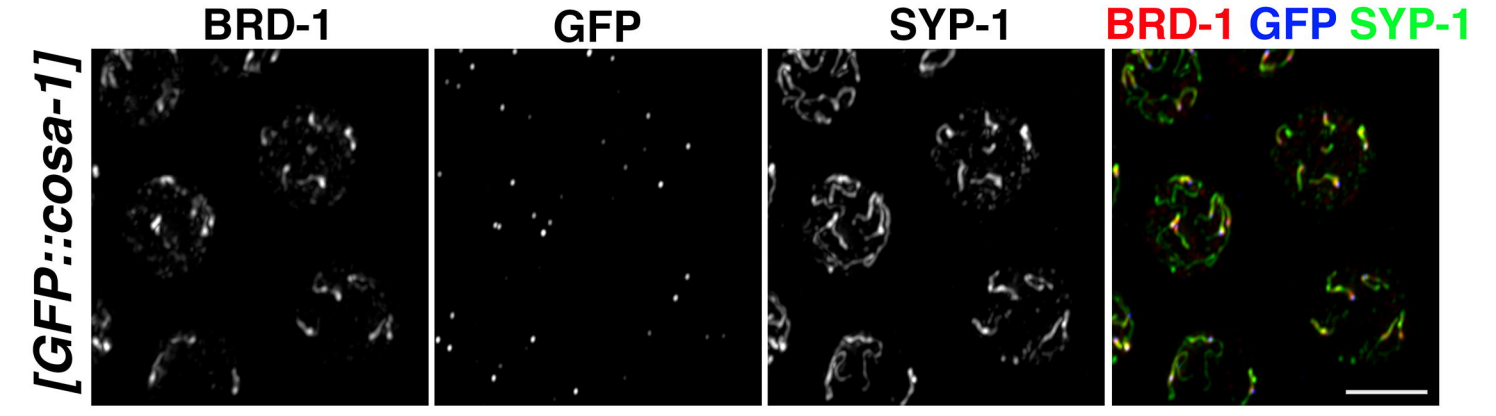
BRD-1
GFP
SYP-1
BRD-1 GFP SYP-1
[GFP::cosa-1]

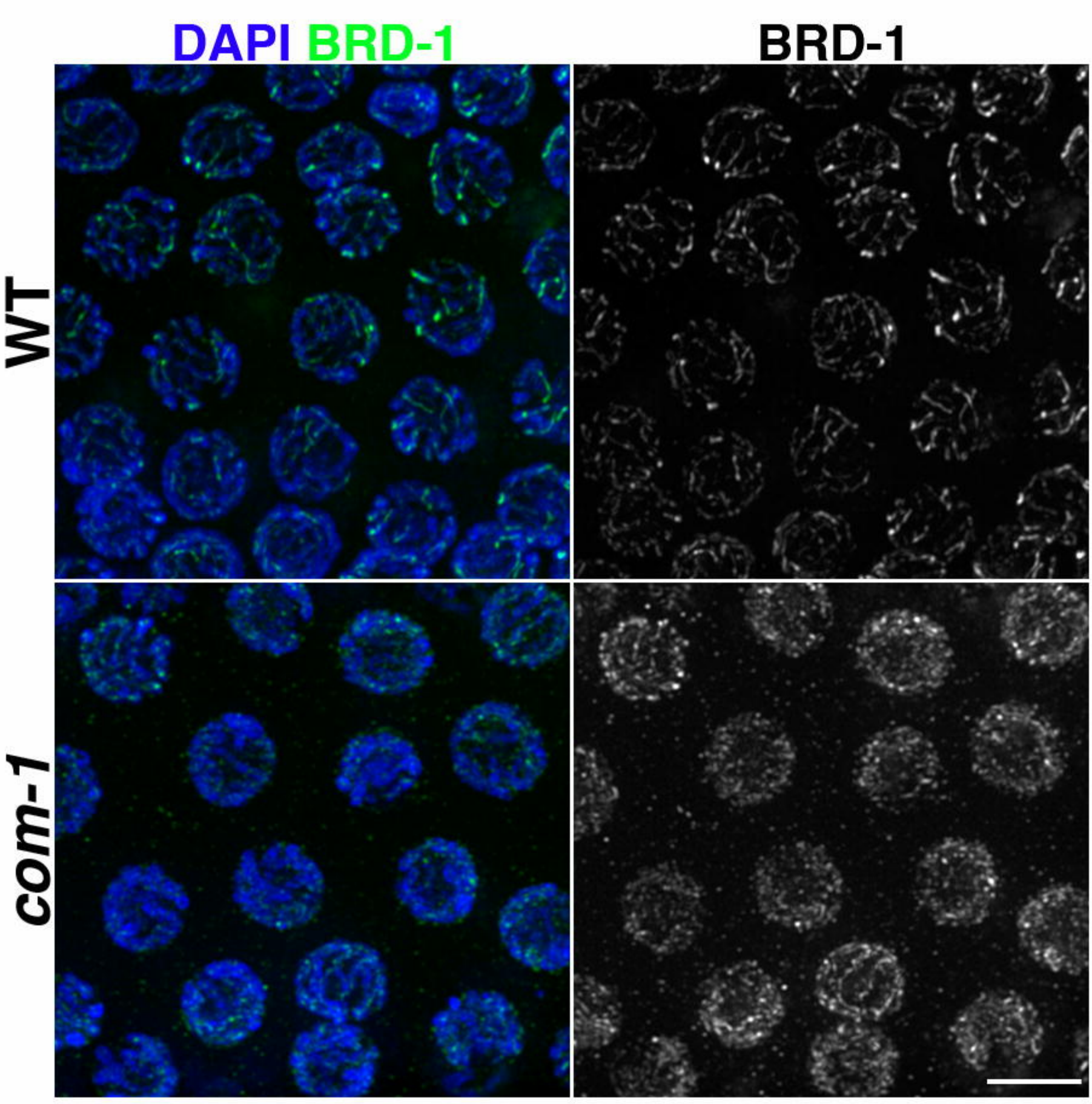
DAPI BRD-1
BRD-1
WT
com-1

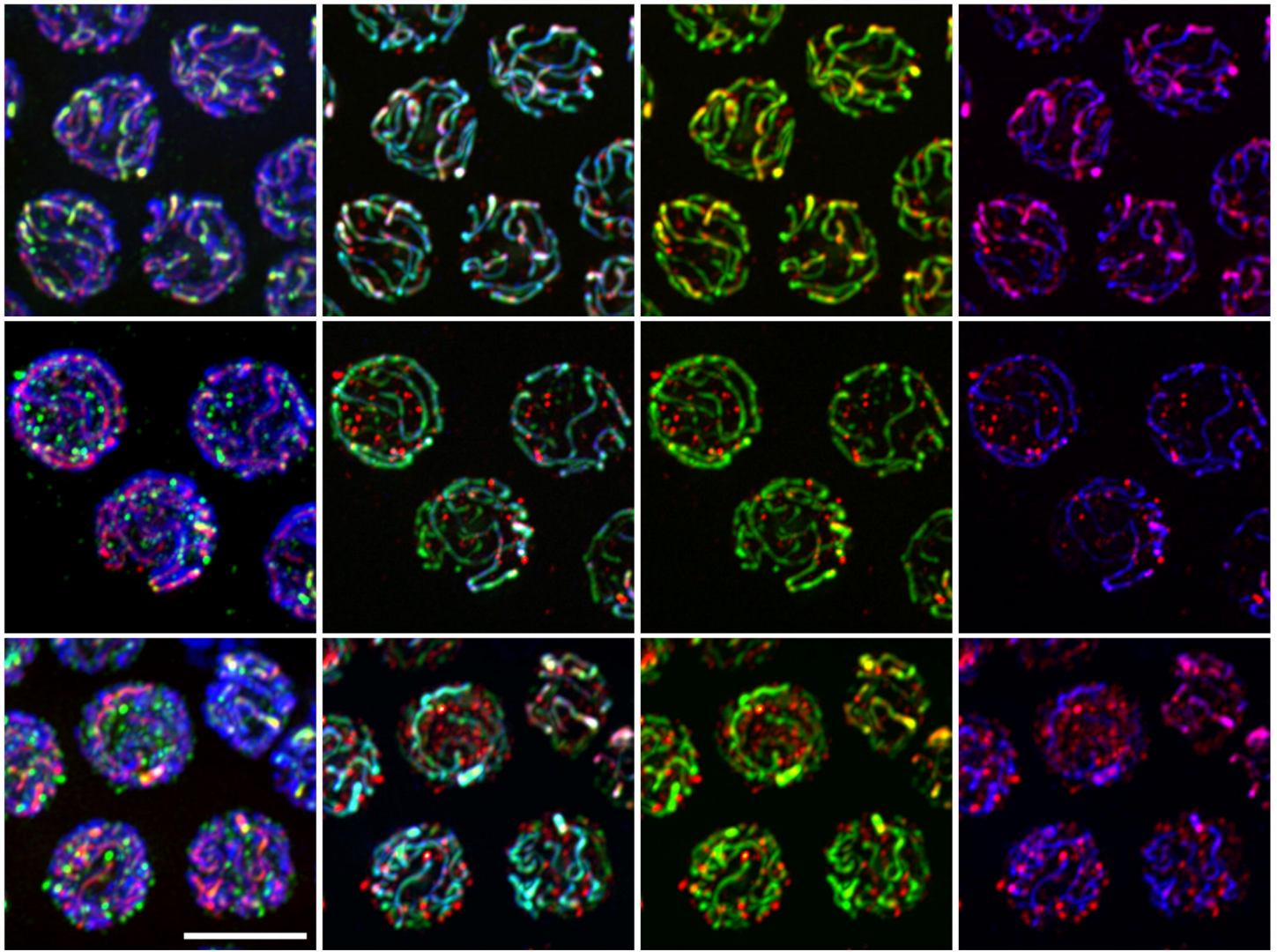
DAPI
BRD-1 HTP-3
SYP-1
BRD-1 HTP-3
BRD-1 HTP-3
BRD-1 SYP-1
WT
htp-1(gk174)
prom-1(ok1140)

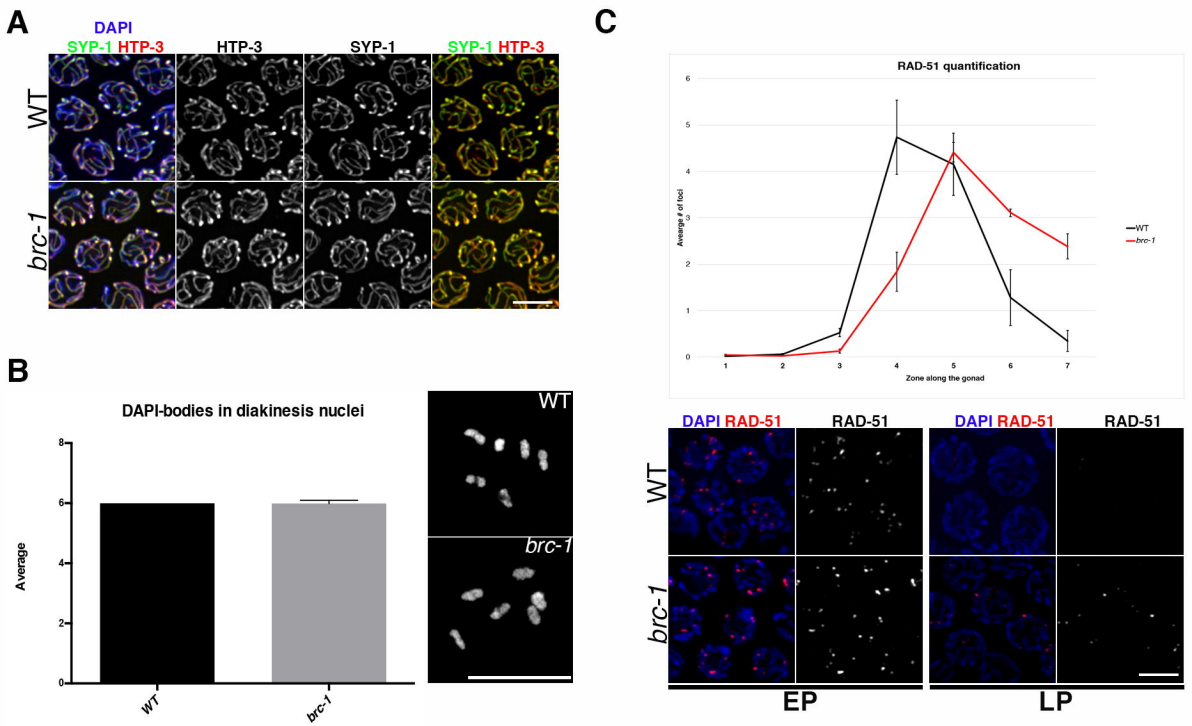
A
DAPI
SYP-1 HTP-3
HTP-3
SYP-1
SYP-1 HTP-3
WT
brc-1
B
DAPI-bodies in diakinesis nuclei
Average
WT
brc-1
C
RAD-51 quantification
Average # of foci
Zone along the gonad
WT
brc-1
DAPI RAD-51
RAD-51
EP
LP

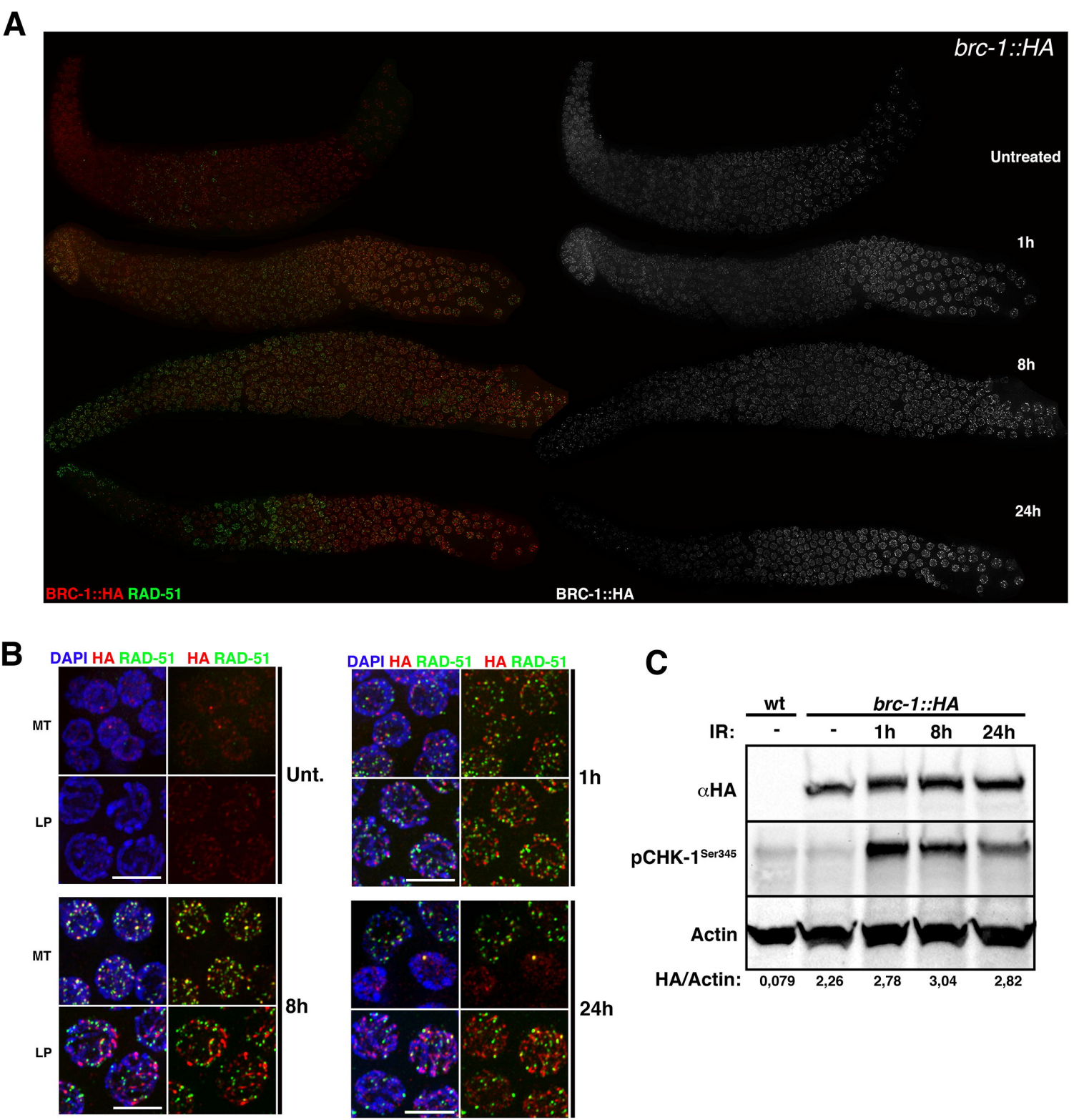
A
brc-1::HA
Untreated
1h
8h
24h
BRC-1::HA RAD-51
BRC-1::HA
B
DAPI HA RAD-51
HA RAD-51
MT
LP
Unt.
1h
8h
24h
C
wt
brc-1::HA
IR:
-
-
1h
8h
24h
αHA
pCHK-1 Ser345
Actin
HA/Actin:
0,079
2,26
2,78
3,04
2,82